Atmospheric Pressure Plasmas at the Liquid Interface

Martin Blake

MSc by Research

UNIVERSITY OF YORK

Department of Physics

January 2014

Abstract

The use of non-equilibrium atmospheric pressure plasmas for medicinal and biological applications has shown great promise. Possibilities exist for potential cancer therapies as well as sterilisation and wound healing. A fundamental understanding of the plasma chemistry is important to the further development of these applications. Of particular importance are the chemical kinetics and energy transport mechanisms at the liquid interface. The aim of this work is to obtain measurements of the important reactive neutral species in this region in order to better understand and control the plasma chemical environment. Direct observation of free radicals is complex due to their very short lifetimes. Spin trapping is used to selectively convert unstable radicals to persistent ones, which are then detected by electron paramagnetic resonance (EPR) spectroscopy. The interaction between a kHz dielectric barrier discharge (DBD) plasma jet (operated using a helium feed gas and molecular gas admixtures) with liquids, gels and single layers of organic compounds are investigated and presented in this piece of work.

Contents

List of Figures

List of Tables

Acknowledgements

Declaration of Authorship

I hereby declare that the work presented in this thesis is original and written solely by the author.

Chapter 1

Introduction

In 1928 Irving Langmuir coined the term plasma from its similarity with the plasma fluid found in the human body's vascular system [1]. The existing model for the 3 states of matter consisted of solids, liquids and gases, however if a gas is ionized through an additional energy input e.g. E-field induced process then a plasma is formed and the resultant state is referred to as the fourth state of matter. The degree of ionisation of a gas is the ratio of the number density of ions to the total number density of particles (neutrals and charged particles), and can range from a fully ionised state such as the sun to a partially ionised state as formed in the technological plasma used in this research.

The quasi-neutrality of a plasma states that the number density of positive and negative charges is the same which means that on a macroscopic scale the plasma is free of an overall electric field; however on a micro scale the plasma has a variety of electric field strengths between particles. Technological plasmas fall into either the thermal or non-thermal regime, the latter being investigated in this research. Thermal plasmas are defined by the plasma bulk being in thermodynamic equilibrium, with the electrons, neutrals and ions at the same temperature represented in 1.1.

$$T_{electrons} = T_{ions} = T_{gas} \tag{1.1}$$

Non thermal plasmas have a high electron temperature (1-4 eV), however energy transfer to the heavier neutrals is not efficient due to the large mass difference therefore leaving the overall plasma state at room temperature, since the background neutral gas is the dominant component. This is a unique delivery system of high temperature chemistry consisting of high radical densities in an otherwise room temperature environment, which is impossible to achieve otherwise.

$$T_{gas} \approx T_{ions} << T_{electrons} \tag{1.2}$$

The use of atmospheric pressure plasma jets (APPJ) such as the dielectric barrier discharge (DBD) kHz setup and radio-frequency (RF) jets have increased in popularity dramatically over the past decade due to huge promise for potential in the fields of healthcare technologies and various other applications within industry e.g. material modification, coatings, deposition and etching as used in the semiconductor industry, as well as on a nanoscale [2]. Understanding of the gas phase chemistry in atmospheric pressure non-thermal plasmas has advanced significantly in recent years, but the transition between the gas and liquid phase, present in many applications, is still not well characterised. This is of great interest as understanding the stages of liquid phase chemistry and the behaviour of radicals under various plasma setups and feed gas mixtures will help in improving control over the plasma's reactive species. Interpreting the chemistry that reaches and enters the liquid will help to optimise conditions for biological treatment.

The micro atmospheric pressure plasma jet used in this study has been extensively studied by experiment and simulations; although it may not necessarily be the most effective design when it comes to treating biological samples due to the electrodes electric field operating perpendicular to the flow of gas resulting in the confinement of charged species. Alternatively the kHz plasma jet has had some positive results in surface treatments such as sterilisation [3]. The motivation for helium as a primary gas is because of its low density and high mean free path. One of its key properties is a high thermal conductivity resulting in a plasma that remains at room temperature. Allowing for direct biological sample treatment, neutral components in the plasma are also of key importance in keeping the overall temperature down [4]. An oxygen admixture was chosen to supply high densities of reactive species [5]. Using electron paramagnetic resonance (EPR), analysis of the plasma treated samples will enable the refining of the reactive chemistry produced at the liquid interface. The purpose behind this research "Atmospheric pressure plasmas at the liquid interface" is to better understand how the plasma reacts with different interfaces. The role that liquids and solids play and whether it is the neutrals, metastable or free radicals that can truly enter the liquid bulk and become effective at treating wounds or killing cancerous cells. The interaction of two different plasma jet designs with liquid and biological samples will be contrasted and presented. This will highlight the plasma effectiveness when treating biological samples in liquids.

The plasma chemistry of interest is based at the liquid surface and appears in the form of surface bombardment, a key experiment will be to understand the overall strength of the reactive chemistry present at the liquid interface and into the body of liquid.

Observations of flow mechanisms that may be present and whether they are due to a thermal or feed gas process.

This thesis will take the following structure; Chapter 2 will consist of a literature review of related plasma applications and state of the art results, as well as techniques used to detect and manipulate radicals. Chapter 3 will show details of the plasma sources used throughout the investigation. Chapter 4 is a summary of the results. Chapter 5 is a conclusion with suggestions for future work.

Chapter 2

Atmospheric pressure plasmas at the liquid interface

2.1 Key plasma characteristics

When comparing non thermal atmospheric pressure plasmas to more conventional non thermal plasmas produced at low pressure there are some benefits; with no requirement for vacuum apparatus, an open system design and operation at ambient atmosphere allowing for direct treatment of biological matter. To generate and sustain a technological low temperature plasma an electric field is applied to a neutral feed gas, in this work helium was used, the free charges are accelerated and collide with atoms and molecules in the gas, this creates an avalanche of charged particles that is balanced and the plasma jet is ignited and sustained [6, 7]. In this investigation, two different electrode configurations were used, which will be discussed in more detail later. Briefly the first being an RF atmospheric pressure plasma jet, which has electrodes such that the gas flow is perpendicular to the electric field. The second is a relatively high voltage kHz dielectric barrier discharge (DBD) plasma jet which has the electric field parallel to the flow of gas allowing for electric fields to be present in the plasma jet and thus also relevant for the surface interaction. The DBD plasma jet configuration will be alternated between a pulsed and sinusoidal power supply.

2.2 Plasma gas-phase chemistry

To help the understanding of plasma-chemistry interactions with biological systems, an understanding of the plasma chemistry within a less involved environment is required.

All the plasma sources will be used in similar conditions and a large proportion of the work carried out in this project will examine a deionised water environment to help simplify the chemistry. This will evolve into work with media to simulate a biological environment. The micro-APPJ has been well studied both experimentally and via simulations concerning gas temperatures, electron properties with a variety of global chemical kinetic models to suit [8–12]. Previous studies mainly apply to the gas phase, so this work will focus on plasma surface interactions.

The key chemistry involved is highly dependent on the ratio of oxygen or nitrogen added to the feed gas, which plays a key role in determining the reactive species produced. Reactive oxygen species (ROS) and reactive nitrogen species (RNS) are commonly referred to as RONS [13]. These species have been shown to play key roles in biomedicine and sterilisation [14–16].
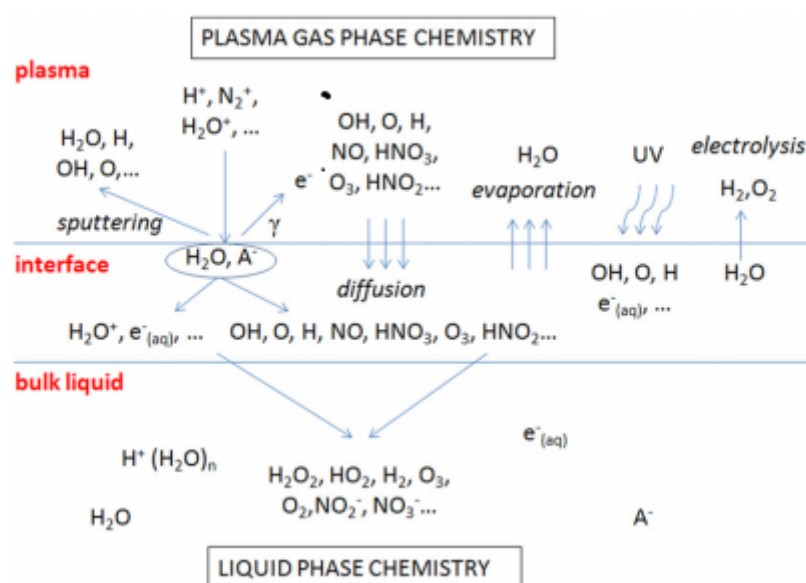
FIGURE 2.1: Key diagram showing the reactive species at various stages of plasma chemistry in a gas and a liquid environment [17]

Figure 2.1 gives potential pathways of nitrogen and oxygen reactive species relevant to the liquid or gas phase, the work carried out in this thesis is concerned mainly with oxygen and its associated reactive chemistry, however with local atmospheric interaction, nitrogen species will play a role in the interaction at the interface [18].

2.3 Reactive species

The reactive chemistry generated within the plasma initiates complex and interesting chemistry at the surface and within a biological environment. These interactions depend on the various parameters including gas admixture, environment and the state of the

sample. In diagram 2.2 the various stages of plasma production and sample treatment outline the species that may be responsible for biological interactions. The electron temperatures are much higher in comparison with the ions and sustain the plasma through external electric fields and collisional processes with the background gases [13]. It is during this process that any oxygen or nitrogen admixtures will be dissociated by the hot electrons creating the reactive chemistry.
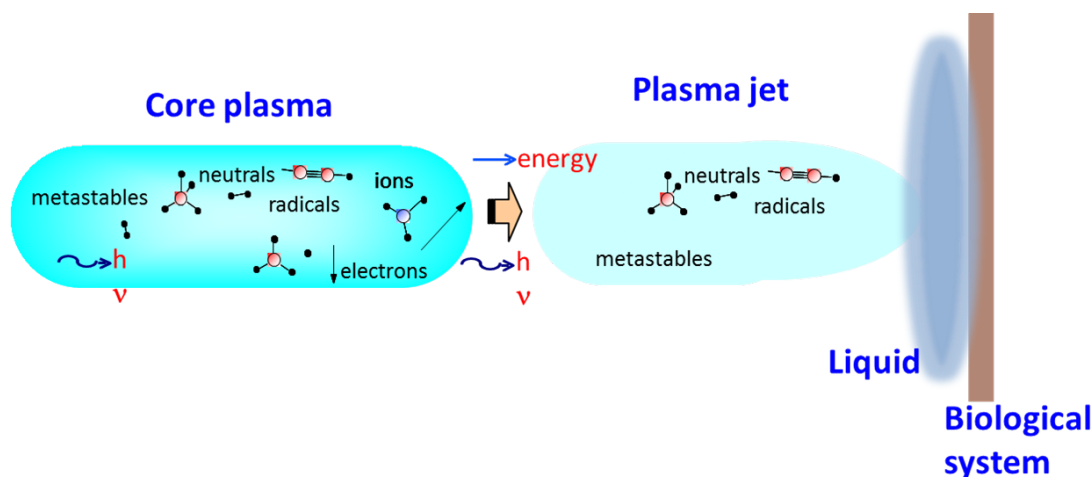
FIGURE 2.2: Reactive species produced in an RF plasma, charged species are confined to the electrode region, however the complexity of the chemistry is apparent

The species studied in this work will concentrate on those produced in a helium plasma with oxygen admixture, a sample of which include hydroxyl radical ($OH\cdot$), superoxide anion radical ($O_2^{\cdot-}$), ozone (O_3), singlet delta oxygen ($O_2(a^1\Delta_g)$) and atomic oxygen (O).

The idea of introducing an additional oxygen admixture is due to the various products of oxygen. With the addition of a varying number of electrons to oxygen the products can vary significantly, ranging from superoxide anion radical $O_2^{\cdot-}$ which is produced by the addition of a single electron to oxygen then onto hydrogen peroxide H_2O_2 with the further addition of an electron. 3 electrons removed from oxygen and it results in $OH\cdot$ and a fourth electron gives a product of H_2O [19]

2.3.1 Superoxide radical

There is much interest in $O_2^{\cdot-}$ as it has the potential to alter various functions within the cell and affect cell signalling, which can lead to cell death. A key step in this process has been shown to be dismutation of $O_2^{\cdot-}$ into H_2O_2 [20, 21]. $O_2^{\cdot-}$ is also known to play a key role in the inactivation of bacterial cells within a liquid environment [22].

$$O_2^{\cdot-} + O_2^{\cdot-} + 2H^+ \rightarrow H_2O_2 + O_2 \tag{2.1}$$
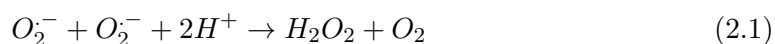
Equation 2.1 is the dismutation of $O_2^{\cdot-}$ in an aqueous solution, this results in an oxidisation to O_2 and a reduction to H_2O_2.

2.3.2 Hydrogen peroxide

Hydrogen peroxide H_2O_2 can be detected by various detection kits and other colorimetric techniques, generally these colorimetric techniques offer better sensitivity and allow for accurate calibration to be predetermined. [23] Oehmigen et al have previously observed an increase in H_2O_2 following indirect treatment of a liquid.[24]. As outlined by Forman et al [25] H_2O_2 production can be a result of the dismutation of $O_2^{\cdot-}$ as shown in equation 2.1.

2.3.3 Hydroxyl radical

In the plasma surface interaction where the plasma effluent is in direct contact with the surface $OH\cdot$ radicals are formed through dissociation of water molecules [16, 26]. The level of $OH\cdot$ produced in the gas phase will also contribute to the EPR signal strength therefore care must be taken when differentiating between the overall radical strength of the two contributions. This radical is readily produced and thought to contribute in the death of cancerous cells [13], $OH\cdot$ is a very strong oxidising agent and is the most reactive known radical and is therefore well suited for analysis by spin trapping.

$$H_2O \rightarrow H + OH \tag{2.2}$$

Equation 2.2 is the dissociation of water resulting in products relevant for biomedical applications [13].

2.3.4 pH

A significant part of the change in pH and sterilisation derives from an interaction between water ions and water molecules. The product is a Hydronium ion (H_3O^+) [27]

$$H_2O^+ + H_2O \rightarrow H_3O^+ + OH\cdot \tag{2.3}$$

Equation 2.3 states the process that results in the acidification of the plasma treated water, $OH\cdot$ is also a product.

In experimental conditions (3.6) when treating the H_2O sample an acidification was observed. It has been noted that pH is important for the inactivation of bacteria, certain pH values promote bacterial inactivation while values above ~ 4.7 show little or no effect when plasma treated [22, 28].

2.3.5   Singlet delta oxygen

Singlet delta oxygen is another generated species that has been shown to have significant impact in biological systems and has been shown to be important in causing oxidative damage after plasma exposure [29]. One of its key features is a relatively long gas phase lifetime of 75 min [30]. This doesn't take into account how the chemistry changes once it has been introduced to a liquid interface.

2.3.6   Ozone

The work with sterilisation due to an ideal pH region is dismissed by Pavolich et al [31] as their research concludes the main sterilisation process can be attributed to ozone, and not to a lowering of the pH. The study showed that treatment occurring over a much shorter time scale typically 5 s with low a plasma operating powers 0.2 Wcm^{-2} achieved the best sterilisation results. This technique does require thorough mixing of the sample during treatment.

2.4   Physics of Electron Paramagnetic Resonance (EPR)

This method is ideal for studying the reactive chemistry produced in a plasma treated liquid sample with one or more unpaired electrons, the principles of this technique are based on the Zeeman split energy levels as seen in figure 2.3 due to the varying spin of the electron, this is produced through an external magnetic field and the resonant absorption between the two energy levels is recorded [32].

Figure 2.4 is a picture of the model used throughout this experiment; EPR measurements were carried out at room temperature with a JEOL X-band spectrometer (JES-RE1X)

EPR spectroscopy is a technique used to detect free radicals and paramagnetic species. The important aspects of EPR in relation to the electron and its behaviour can be
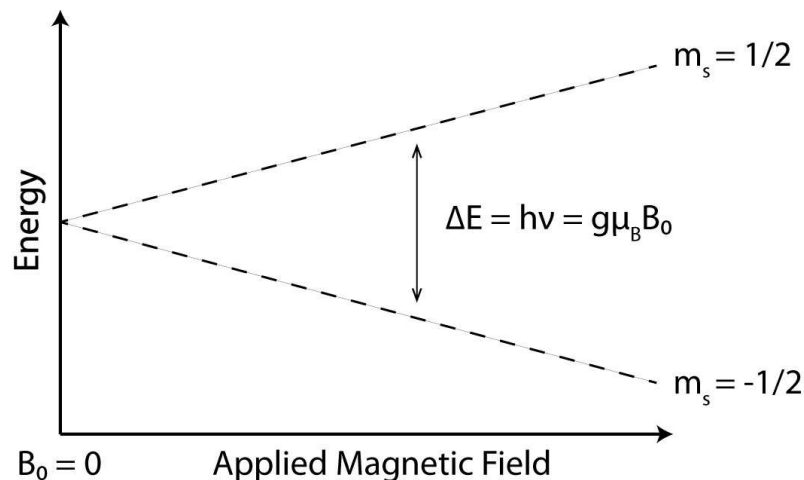
FIGURE 2.3: Zeeman-split energy levels.

derived from the electrons angular momentum (spin S) and the associated magnetic momentum μ_e giving:

$$\mu_e = -g_e \mu_B S \tag{2.4}$$

Where the g factor for a free electron is 2.0023 and μ_B is the Bohr magnetron.

EPR works by applying an external magnetic field across a sample placed between the two electromagnets. This aligns the magnetic moment of the electrons in the sample either parallel or anti parallel to the applied field. This creates two energy states, the highest coming from the positive spin of the electrons magnetic moment and the lower coming from the negative. When the frequency and magnetic field are optimised electrons in the lower spin state are excited into the upper to produce an EPR resonance. With EPR spectroscopy the option exists to either vary the photon frequency while keeping the magnetic field constant or to keep the frequency fixed and vary the magnetic field. In this research the frequency was maintained at 9.1 GHz and power at 5 mW. This puts it in the microwave region, and the separation of the two states of $m_s = \pm\frac{1}{2}$ increase linearly with the magnetic field B.

$$\Delta E = -g_e \mu_B B \tag{2.5}$$

These two energy levels are specific values due to the Zeeman Effect; the graph also shows the differences between the two energy levels are proportional to the magnetic field strength. The process of preparing samples started by sealing the glass capillary tubes with a Bunsen burner however this was observed to allow the glass to conduct heat

FIGURE 2.4: JEOL EPR spectrometer as used in this research.

into the sample and potentiality distort the chemistry. So this was changed to sealing the glass capillary tubes with putty instead.

2.5   Spin traps

The three main spin traps used throughout the project were (Alpha-phenyl N-tertiary-butyl) PBN, DMPO and DEPMPO along with various other chemicals used during the duration of the project, each filling a specific set of requirements. The spin trapping process works to extend the lifetimes of short lived radicals and this allows for the radicals to be detected and observed through the means of an EPR spectrometer.

$$Radical(R\cdot) + SpinAdduct(SA) = SpinTrap(ST) \tag{2.6}$$
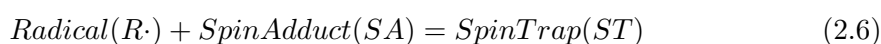
The conditions for spin trapping to be successful are that the spin traps themselves must not be involved in any side reactions that will create paramagnetic species not relevant to the final chemistry. They must be stable and the addition of spin trap to the radical must be a fast process, otherwise interference from non-relevant species will occur [33]. There are two main types of spin traps, nitrone and nitroso both of which have nitroxide radical products, both of which are stable. The structures of a nitroso and nitorne spin trap along with the spin adduct or nitroxide radical figures 2.5 and 2.6.
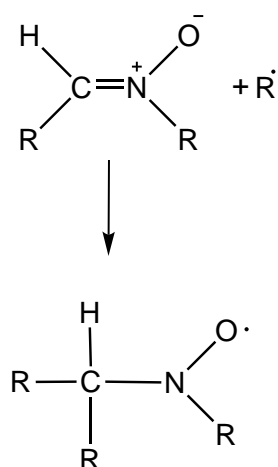
FIGURE 2.5: Nitrone spin Trap
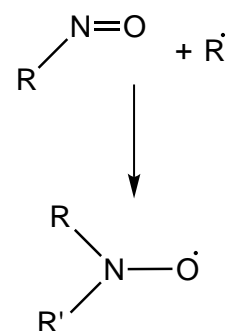
FIGURE 2.6: Nitroso spin Trap

The critical difference between the nitrone and nitroso spin traps is the point at which the radical attaches itself to the spin trap. For example with a nitroso spin trap the radical attaches directly to the nitrogen in the compound, this allows for greater influence on the EPR spectra, which usually creates specific hyperfines for the different radicals, however the disadvantage being that the adducts are usually less stable and more toxic to cells, with large instabilities associated with oxygen centred radicals [21]. For this reason nitroso spin traps were not used in this research. Nitrone spin traps work slightly differently and have the radical attach to the carbon element of the spin trap compound, this does give a much more generic spectrum, but it is still possible to determine which radical has been trapped. All three of the spin traps used in this investigation are nitrone.

2.5.1 Nitrone spin traps and their properties:

Some of the key properties of the spin traps used in this study are listed below:

Alpha-phenyl N-tertiary-butyl (PBN)

- PBN is readily available, cost effective and can be analysed in vivo.

- Minor issues when extracting hyperfine values from the data as they are all very similar values.

PBN
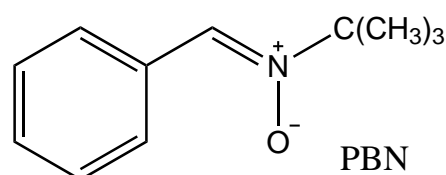
5,5-dimethyl-pyrroline N-oxide (DMPO)

- Stroger $OH\cdot$ adducts due to rate constants and general sensitivity.

- DMPO reaction rates for $OH\cdot$ and $O_2^{\cdot-}$ are $> 10^9\mathrm{M}^{-1}\mathrm{s}^{-1}$ and $< 10^2\mathrm{M}^{-1}\mathrm{s}^{-1}$ respectively [21].

- Ability to differentiate between $OH\cdot$ and $O_2^{\cdot-}$ due to the addition of DMSO.
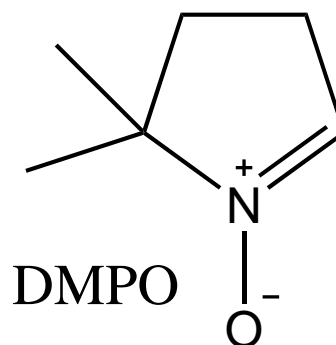
5-(Diethoxyphosphoryl)-5-methyl-1-pyrroline-
N-oxide (DEPMPO)

- DEPMPO has rate constants in the same scale as DMPO however it has $O_2^{\cdot-}$ adducts that are approx. 15 more stable than that of the DMPO $O_2^{\cdot-}$ adduct [34].

- A large number of radicals are trapped and therefore spectra requires detailed analysis.
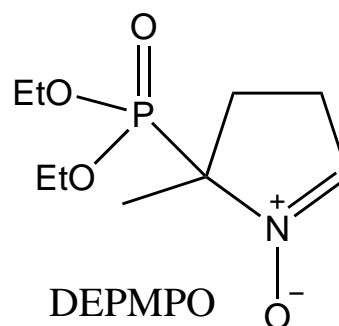
Dimethyl sulfoxide (DMSO)

- DMSO was used initially to confirm the presence of $O_2^{\cdot-}$ in a DMPO solution.

- DMSO is introduced to scavenge the $OH\cdot$ radical, as it reacts with DMPO it creates methyl radicals CH_3 which enables $O_2^{\cdot-}$ to be trapped as it has a faster reaction time than the $OH\cdot$ radical [21]. Any $OH\cdot$ detected after this point can be attributed to $O_2^{\cdot-}$ production.

2.6   Free radicals and liquid interface

Figure 2.7 shows the various paths taken by the Hydroxyl ($OH\cdot$) and Superoxide $O_2^{\cdot-}$ radicals once trapped by DMPO. It can be seen that the various life times of the radicals and the ability of the spin traps to retain the radical can vary. 5,5-dimethyl-pyrroline N-oxide (DMPO) has a very stable $OH\cdot$ adduct, however at equal parts of $O_2^{\cdot-}$ and $OH\cdot$ rate reactions are different, and when the two radicals appear in equal concentrations, the

efficiency of O_2^- to form an adduct is much lower than that of $OH\cdot$ [21]. Information on the radical that has been trapped is obtained from the hyperfine splitting of spin adducts [35].

The problem with the O_2^- radical is that it is very unstable and reacts readily with other species to form different chemical species. This leads to the use of spin traps such as 5-(Diethoxyphosphoryl)-5-methyl-1-pyrroline-N-oxide (DEPMPO) as it has a more stable adduct for both the $OH\cdot$ and O_2^- radicals, however it also traps a wide variety of other radicals producing complicated spectra. When observing the comparisons of O_2^- with $OH\cdot$ in an aqueous solution it is much less reactive with non-radicals [36].
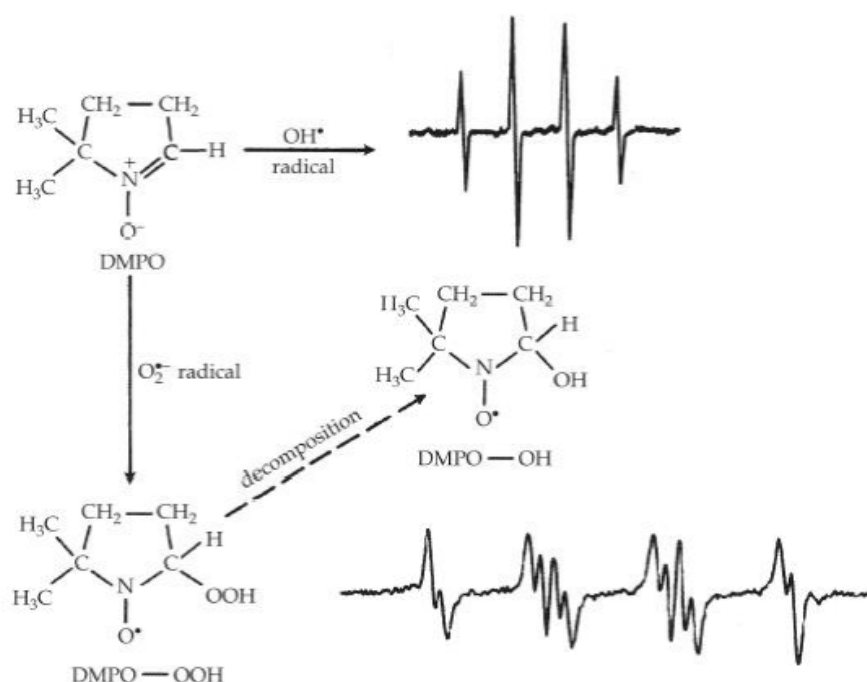
FIGURE 2.7: Shows the pathways of radicals trapped with DMPO spin trap, it has a strong $OH\cdot$ adduct but due to the short lifetime of O_2^- it tends to decompose to $OH\cdot$ eventually [21, 37].

Figure 2.7 shows the spectrum obtained from DMPO when trapping $OH\cdot$ and O_2^- with the relevant EPR spectra, it also emphasises the likelihood of O_2^- decomposing back to an OH form due to the sensitivity of trapping O_2^-.

2.7 Fourier Transform Mass Spectrometry (FTMS)

The effectiveness of using atmospheric pressure plasmas for cleaning a gold coated surface was also investigated. The motives for using the plasma to clean the organic monolayer and matrix off the substrate is that the current method uses a piranha solution that

causes significant damage to the gold surface and requires the plates to be replaced every 3 wash cycles. Gold is used as the coating as it has a strong bond with the sulphur in the monolayer. The cost of each plate is approximately £20 therefore a financial motive for an alternative method is justified. Diagnostic benefits for the plasma will come from analysing plates that have been treated with various admixtures, whether it has just an organic monolayer or a matrix as well and which molecular gas admixture or plasma setup has the greatest cleaning impact.

Behind Fourier Transform Mass Spectrometry is the determination of the mass to charge ration (m/z) of ions. It is based around the excitation of these ions from trapped states to one of a significantly larger cyclotron radius; this only occurs if the ion does not collide and lose its energy. Once the larger ion radius has been achieved the excitation field is replaced by all the ions moving in phase. Ions of the same mass to charge ratio group up and undergo cyclotron motion together they pass by the electrodes which lie parallel to the magnetic axis and create an image current as shown in figure 2.8 [38].
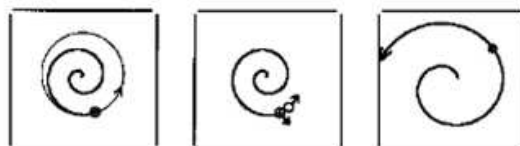
FIGURE 2.8: Excitation process of an ion in an FTICR [39].

Chapter 3

Experimental setup and diagnostics

3.0.1 KHz Plasma operating conditions

This research project was based largely on this particular plasma jet; its design allows the user to point the jet precisely on a specific treatment area. Its design is relatively simple and the gas flow rate can be altered using mass flow controllers. Alternatively if the limit of the mass flow controllers has been reached it can be further manipulated by changing the internal diameter of the quartz glass tube. In the initial setup stage the glass tube was standard Pyrex glass, because of the nature of the sinusoidal power supply it appeared to build up a level of heat around the powered electrode and subsequently damage the Pyrex glass. Quartz glass was used due to it being more thermally resistant. The nature of the atmospheric pressure plasma design and lack of vacuum equipment reduce the list of components needed and improves the cost effective nature of this particular design. A few key issues with the increased interactions from atmospheric gas components complicates the chemistry, and keeping the relationship of voltage to feed gas flow rate carefully controlled avoids any heating or sample evaporation that can affect final results. The key reproducibility factor is to ensure consistent operation with the same voltage and frequency making sure any changes are recorded or anomalies eliminated.

A significant factor with the high voltage sinusoidal power supply was the fluctuation in output voltage this was measured at 17 % using a Lecroy high voltage probe and Lecroy wavejet oscilloscope. However for comparison reasons this setup was included in similar experiments run using a 'Megaimpulse' high voltage pulsed nanosecond power supply. Both have identical electrode and quartz glass tube parameters, and attached

to two Brooks mass flow controllers, one calibrated to helium (maximum flow rate of 2000 sccm) and oxygen (maximum flow rate of 50 sccm).
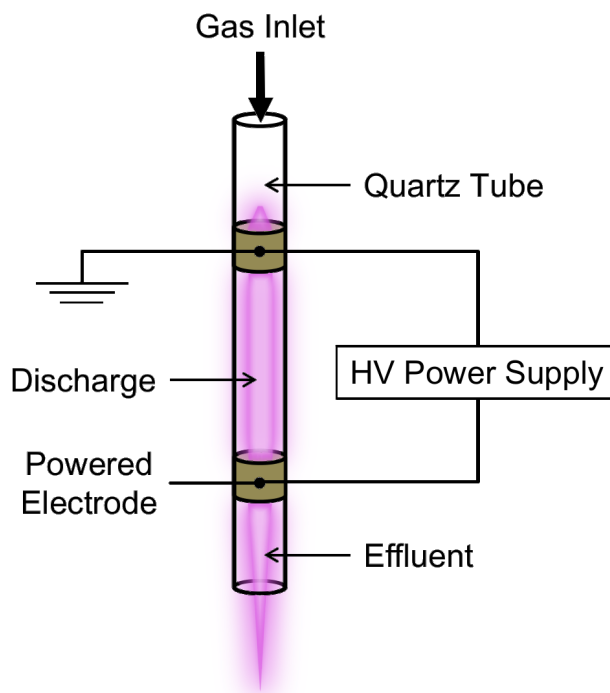
FIGURE 3.1: KHz Plasma jet setup.

Electrode placement is also a key area for refining the plasma properties, all the work outlined in this these experiments had two electrodes one grounded and the other powered with the powered at the bottom of the configuration nearest the plasma effluent as shown in 3.1.

The electrodes consisted of 8 mm wide copper tape, with a 20 mm gap between the powered and grounded electrode and a further 10 mm gap between the grounded electrode and end of the quartz tube. Changing the distances has a large effect on the plasma. The flow rate remained at 2 slm; this also depended on the internal diameter of the quartz tube being used, which remained at 6 mm outer diameter (OD) and 4 mm inner diameter (ID) and a length of 100 mm.

Sustainment in the plasma occurs when a thin ionising channel (streamer) originates in a region of high electric field and continues to propagate. An electron avalanche is created and will develop a self-induced electric field, this is due to the electrons and ions moving in opposite directions (within an externally applied electric field) and thus a space charge region forms. This self-induced space charge electric field can become very large, even allowing the streamer to propagate into regions where the applied electric

field is not sufficient for ionisation to occur. For streamers to continue propagating new free electrons must become available at the tip of the streamer.
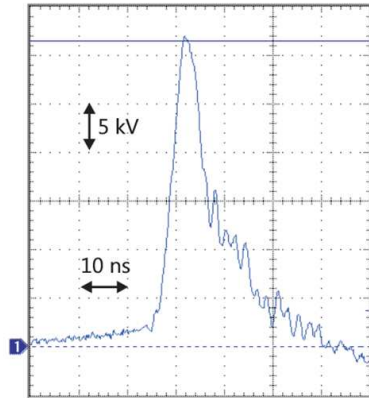
FIGURE 3.2: Typical pulse waveform of the pulsed high voltage nanosecond power supply.
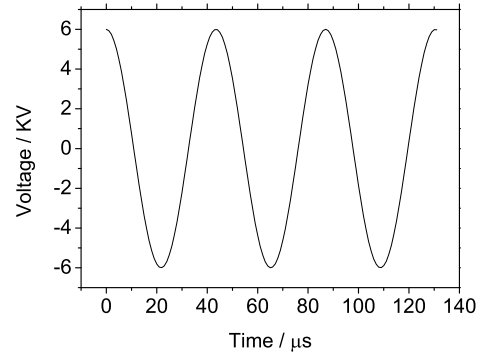
FIGURE 3.3: High voltage power supply with a sinusoidal waveform.

Figures 3.2 and 3.3 show typical waveforms for the different DBD plasma jet power supplies. The jet and electrode configuration is identical in both kHz plasma jets, the differences are in the driving voltage, frequency and waveform. Nanosecond high voltage pulse waveform with a pulse voltage of up to 36 kV and a maximum frequency of 3.2 kHz, one of its key features being a fast rise time of <4 (ns).

The high voltage sinusoidal waveform was operated with a voltage of $5 \rightarrow 10$ kV and at a frequency of $20 \rightarrow 25$ kHz.

3.0.2 Radio Frequency (RF) plasma configuration

The setup of the RF is a more reproducible and stable plasma, the design of the capacitively coupled RF plasma is shown in figure 3.4.
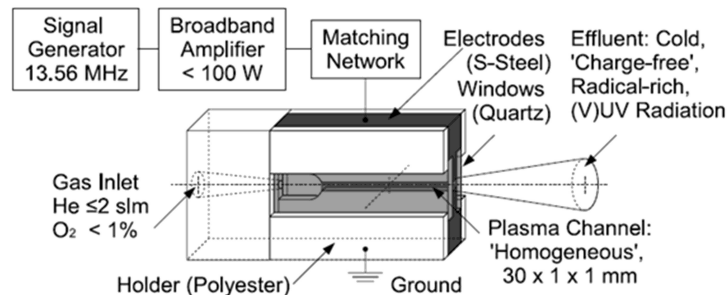
FIGURE 3.4: Radio Frequency (RF) Plasma[40].

A Cesar RF power supply was used and connected to a MFJ-679 matching network, while the gas was supplied through MKS mass flow controllers. A key difference between the design of this plasma setup and the kHz plasma jet is that the stainless steel electrodes run parallel to one another. The quartz glass windows allow for observation throughout experimentation. One electrode is powered and the other grounded, the powered electrode is operated using a signal generator that produces a sinusoidal voltage at 13.56 MHz frequency, in this case the peak to peak voltage is in the order of hundreds of volts. The key sustainment phase is centred on the varying inertia of electrons and ions. Flow rates were between 1 slm and 2 slm helium with oxygen and nitrogen molecular admixtures at varying percentages.

3.1 Diagnostic techniques

The objective of the research was to identify radicals through various diagnostic techniques, which range from simply detecting the presence of radicals to the detailed analysis of their signal strength and distinguishing between the radical types. The first being a simple (N,N-(2-hydroxy-Snitro-1,3-phenylene)bisglutaramide) NPGA compound [41] that contained ammonia and reacted with $OH\cdot$ radical to confirm its presence and strength. The intensity and rate of $OH\cdot$ detection was affected by treatment time and position in relation to the plasma. This also allowed for tests using silica beads and glass wool to be coated in NPGA and positioned inside the quartz glass tube to measure $OH\cdot$ production at the core of the plasma.
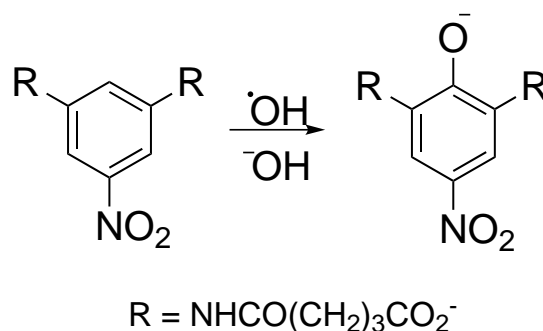
FIGURE 3.5: Chemical process outlining the colour change due to the presence of $OH\cdot$.

Figure 3.5 illustrates the chemical change as $OH\cdot$ reacts with the NPGA to form a yellow compound of varying strength, the experiment was designed to examine the areas within the quartz glass tube during plasma operation that had a greater $OH\cdot$ concentration. The biggest challenge was that the gas flow rate and temperature proceeded to dry the sample and evaporate all the NPGA solution off. This was overcome by introducing

solutions of Glycerol and PEG 450 to decrease the evaporation from heating and gas flow.

3.1.1 pH Monitoring

The variation of pH throughout pre- and post- solution testing will help to understand the treatment environment; a Hanna HO 8424 monitor and HI 1230 probe were used to monitor the liquid solutions at various treatment stages. These results were an exercise in confirming the acidification of the plasma treated liquid, in all cases the deionised water started with a pH of 8 but due to atmospheric influences the pH stabilised at 5.5 slightly below neutral pH before the experiment commenced. This was due to the location of the water relative to the plasma sources, but explains why the starting value is at a pH of 5.5.
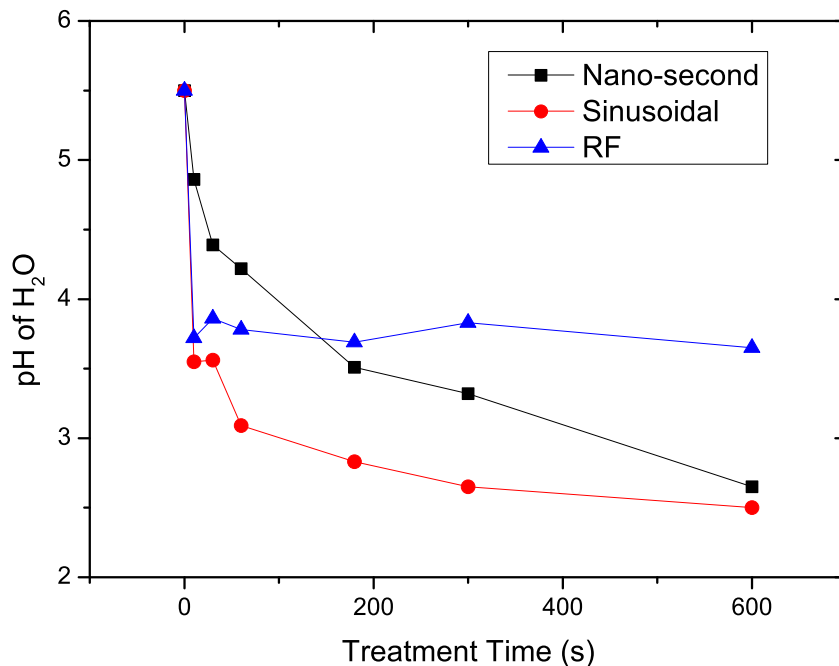
FIGURE 3.6: A variation in pH as a function of time, with a sample solution of H_2O and treatment distance of 12.5 mm for the nano-second and sinusoidal plasmas and 2.5 mm for the RF plasma.

Figure 3.6 shows the acidification of the 1.5 ml of sample liquid over a 10 minute treatment cycle. The Nano second and sinusoidal plasma setups were held 12.5 mm from the liquid surface during treatment while the RF was positioned 2.5 mm from the surface. In conclusion there is a significant acidification that should be considered when treating

biological samples for extended time periods, however it does mean radicals can operate in a variety of pH levels.

3.2 Hydrogen peroxide measurements

There are various methods to test for hydrogen peroxide; this is important when considering plasmas for treatment in a biological environment. A few of the popular approaches are indicator strips, colorimetric methods and titrations. Hydrogen peroxide detection kits that use indicator strips have larger error due to sensitivity issues, the colorimetric method provides a more sensitive hydrogen peroxide concentration measurement using a reference spectrum.

This involves measuring the concentration of coloured compounds in liquids. Titanium (IV) oxalate produces a yellow complex when reacted with hydrogen peroxide that absorbs strongly at 400 nm. Considering the absorbance at a specific wavelength it is possible to determine a variety of unknown concentrations of peroxide. This method allows for samples with relatively low hydrogen peroxide concentrations, the value published states in the 10 μM region.

In this work the calibration data will be taken between 50 μM $\rightarrow$ 2 mM using a UV-Visible spectrophotometer. It was possible to take readings of absorbance intensity and plot a graph against known peroxide concentrations. The concentrations were taken at a series of intervals post plasma treatment as described in section 4.1.3, the chemical reaction showing the process is shown in 3.1.

$$Ti^{4+} + H_2O_2 + 2H_2O \rightarrow TiO_2 \times H_2O_2 + 4H^+ \tag{3.1}$$

Equation 3.1 is the analysis of colorimetric method through H_2O_2 formation.

3.3 Spin trapping, hyperfines and radical lifetimes

The basis of spin trapping is to extend the lifetime of short lived reactive species through a variety of spin traps as mentioned in section 2.5 thus allowing detection and analysis in an EPR spectrometer. Initial results will compare the chemistry from well characterised gas phase chemistry taken using the RF plasma jet [8, 12].

3.3.1 Radical lifetimes

The lifetime of a radical is based on a variety of conditions, firstly an efficient and time effective method for analysing the sample immediately after treatment is crucial due to the radicals rate of reaction. In a spin trap solution radical lifetimes can vary from minutes to hours. For this reason the plasma set up was placed in close proximity to the EPR spectrometer. After treatment the liquid sample was placed in a glass capillary and sealed before placing between the electromagnets of the EPR. Initial testing provided standardised EPR setting which were applied to all samples. The data obtained was analysed in SpecView which allowed for direct comparison of multiple spectra as well as comparison with simulated spectra obtained using hyperfines from the NIH spin trap database. These results were taken using the sinusoidal plasma jet with a helium feed gas and an initial treatment time of 120 s.

Figures 3.7 and 3.8 demonstrate the importance of analysing samples promptly. Figure 3.7 shows 70 μl of a 56 mM DMPO spin trap solution, treated for 120 s. The sample was left for 15 mins before a spectrum was obtained using the JEOL EPR spectrometer. The dominant species are $H\cdot$ and $OH\cdot$, with the strongest signals representing $OH\cdot$.
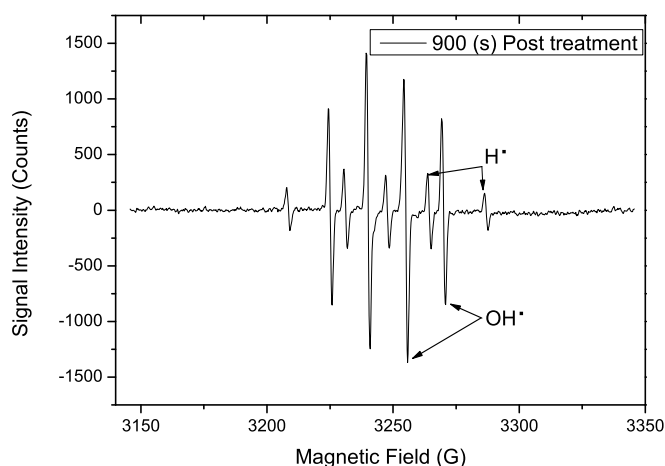
FIGURE 3.7: DMPO spectrum obtained 15 mins post plasma treatment, examining the radical signal strength after predetermined time intervals, the smaller peaks refer to $H\cdot$ radical and the larger to $OH\cdot$.

In comparison figure 3.8 is the same sample that has been left for a further 15 mins to demonstrate reaction rates and how the lifetime of radicals can vary. The signal to noise ratio has evolved and suggests weaker $OH\cdot$. In contrast the signals for $H\cdot$ remain largely unchanged, which confirms $OH\cdot$ to be a more reactive species with a shorter lifetime.
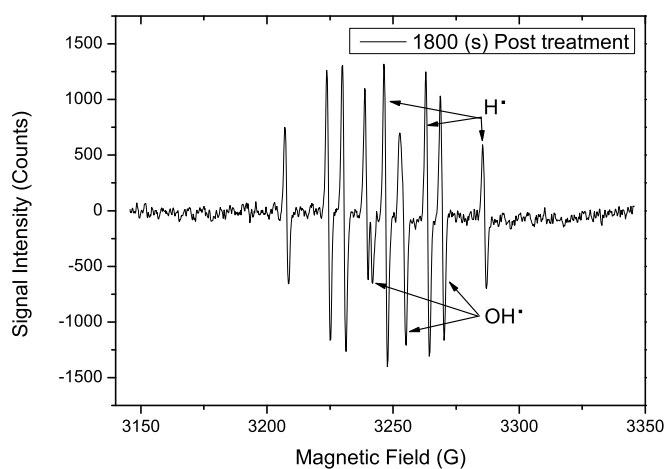
FIGURE 3.8: DMPO spectrum taken 30 minutes after initial treatment of liquid spin trap sample.

3.3.2 Spin traps and associated hyperfines

Figure 3.9 shows trapped radicals of $H\cdot$ and $OH\cdot$, the main features of this spectra are the triplet hyperfine splitting (1:1:1) of the nitroxide adduct. The two variations in spectra are obtained experimentally and through simulation. Noise is not included in the simulated spectrum.
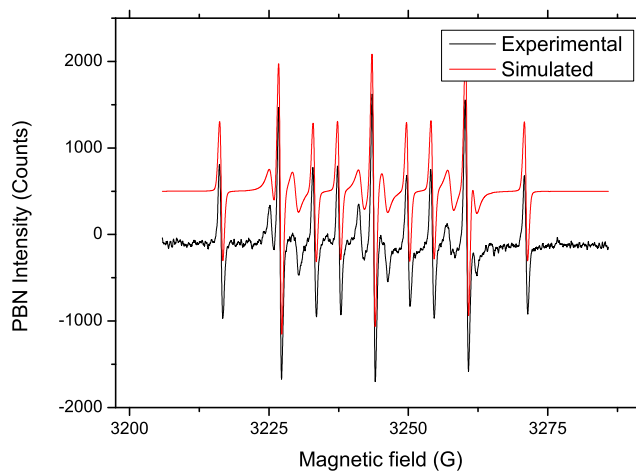
FIGURE 3.9: Experimental and simulated PBN at 56 mM treated for 120 s in a total volume of 70 μl a total distance of 3 mm from the liquid interface.

Figure 3.9 and radical data are extracted using the SpecView software and presented in table 3.1. This data can be matched with published values on the spin trap database to confirm radical presence. In this case distinctive $OH\cdot$ and $H\cdot$ values are confirmed.

Radical	Nitrogen (Gauss)	Hydrogen (Gauss)
$H\cdot$	16.76	10.57 (2H)
$OH\cdot$	16.00	15.09

TABLE 3.1: Hyperfine values in figure 3.9 show the nitrogen and hydrogen quantities detected that represent specific radicals.

The defined nature of DMPO gives these unique and easily identifiable spectra shown in figure 3.10. The kHz plasma jet consistently produced strong signals, this could be due to its placement and gas flow in the direction of the electric field, carrying the reactive species to the liquid interface in comparison with the RF plasma which lacks a defined effluent and overall produced a weaker signal. The results of the extracted hyperfines are displayed in table 3.2 which confirm the presence of $OH\cdot$ and $H\cdot$.
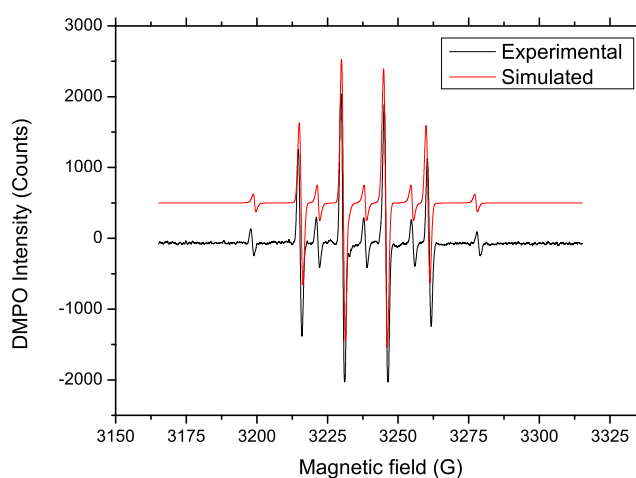
FIGURE 3.10: Experimental and simulated DMPO at 56 mM treated for 120 s in a total volume of 70 μl a total distance of 3 mm from the liquid interface.

Radical	Nitrogen (G)	Hydrogen (G)
$H\cdot$	16.59	22.61 (2H)
$OH\cdot$	14.90	15.09

TABLE 3.2: Hyperfine values for detected radicals in figure 3.10.

With this spin trap the $O_2^{\cdot -}$ radical reaction rate does not compare to that of the $OH\cdot$ radical and therefore the spectrum does not feature this hyperfine. As shown in figure 2.7 the $O_2^{\cdot -}$ can also decompose to form $OH\cdot$ very rapidly. One method to overcome this is to scavenge the $OH\cdot$ radicals.

DMSO is a chemical compound added to the spin trap solution pre plasma treatment, its purpose is to scavenge $OH\cdot$ radicals so the less stable shorter lived radicals are detected without using more sensitive or specific spin traps. The rise in CH_3 spectra confirms a reaction with DMSO and $OH\cdot$ has occurred and drop in the $OH\cdot$ spectrum will be

balanced by a rise in the CH_3 spectrum its presence is confirmed in figure 3.11 with a value included in table 3.3.
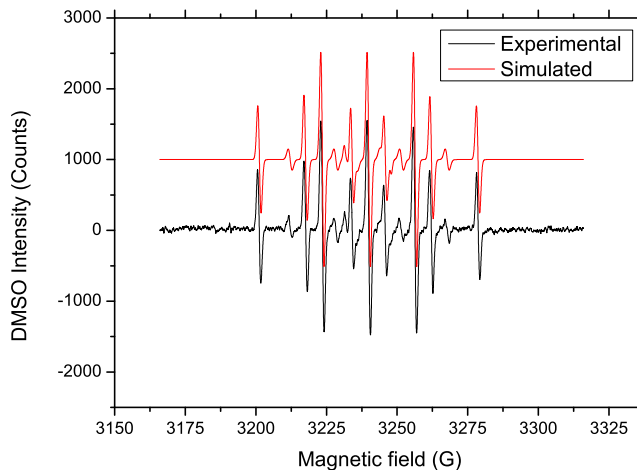
FIGURE 3.11: Experimental and simulated DMPO with a DMSO admixture.

TABLE 3.3: Hyperfine values for detected radicals in figure 3.11.

Radical	Nitrogen (G)	Hydrogen (G)
$H\cdot$	16.40	22.29 (2H)
$OH\cdot$	15.10	14.30
CH_3	16.17	23.24

This is confirmed in figure 3.11 where the $OH\cdot$ has decreased in intensity and the hyperfine for CH_3 has been detected. Varying the DMSO percentage will have a direct effect on the strength of the hyperfines.

The sensitivity of DEPMPO, and its ability to trap a wide variety of radicals can be observed in figure 3.12. Most are broadly well characterised and can be obtained from the spin trap database. However the hyperfine values are very similar so care must be taken when analysing DEPMPO spectra.

Radical	Nitrogen (G)	Hydrogen (G)	Phosphorus
$H\cdot$	15.39	20.90 (2H)	50.61
$OH\cdot$	14.04	13.58	47.20
$O_2^{\cdot-}$	13.40	9.56	51.13

TABLE 3.4: Hyperfine values for detected radicals in figure 3.12.

DEPMPO confirms the presence of $O_2^{\cdot-}$ when plasma treating a liquid with an oxygen admixture, the hyperfine values were compared with the trap database for validation. The $OH\cdot$ hyperfines are weaker in figure 3.12 suggesting the previous data signal strength was partially constructed from the decomposed $O_2^{\cdot-}$ radical due to spin trapping with DMPO.
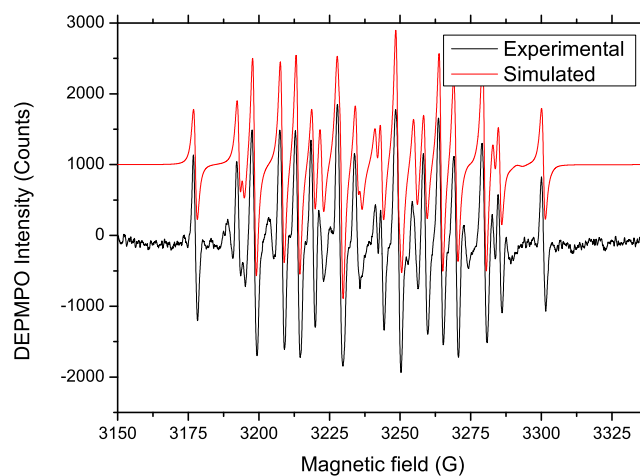
FIGURE 3.12: Experimental and simulated DEPMPO at 56 mM treated for 120 s in a total volume of 70 μl a total distance of 3 mm from the liquid interface.

3.4 Self-Assembled Monolayers

This work allows for better understanding of the reactive species post treatment in a single layer of organic molecules known as a self assembled monolayer (SAM). This work is stimulated by the surface cleaning of gold-coated plates that are analysed using matrix assisted laser desorption ionisation (MALDI), the current technique uses a piranha solution of sulphuric acid H_2SO_4 and hydrogen peroxide H_2O_2 which is very corrosive for the gold surface and leaves it unusable after three washes. Plasma treatment could provide a solution to clearing the SAM and increasing the lifespan of the gold surface. First an optimum admixture and plasma set up needs to be identified

Figures 3.13 shows two sets of spectra pre and post RF plasma treatment. The results are positive in terms of clearing the m/z 861 peak, this indicates the SAM has been cleared and there is a greater possibility of re-spotting another SAM. Both oxygen and nitrogen will be tested and analysed.

The next step is to identify the ideal gas and admixture percentage and look at which plasma supply provides a damaging method for cleaning the plate wells.
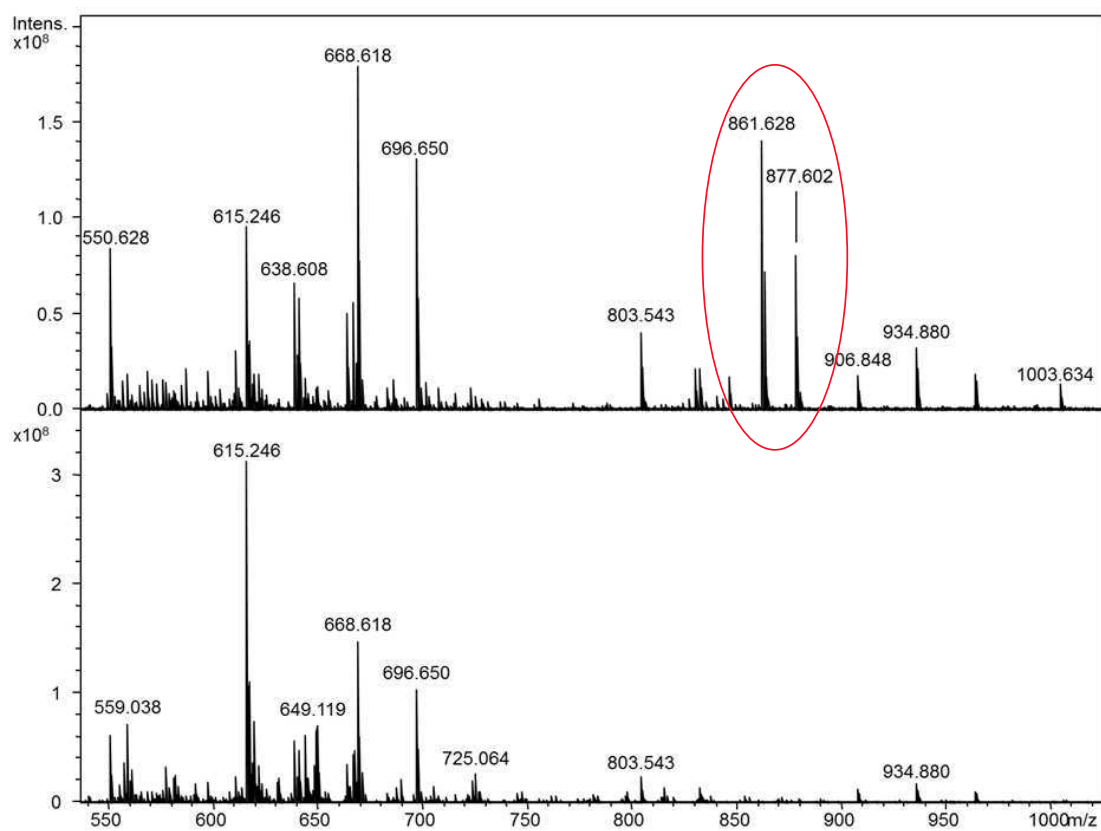
FIGURE 3.13: MALDI mass spectrum obtained on a Bruker solariX of the wells cleaned with an RF plasma operating with 0.1 % nitrogen admixture. Top is a 90 s treatment, bottom is a 180 s well treatment time

Chapter 4

Results

4.1 Characterising and defining important plasma parameters

Initial data was required to produce a model that can be applied to all experiments with the same plasma design and feed gas. Data was obtained using the pulsed nanosecond plasma jet to determine the stability and reproducibility of the hydroxyl radical signal thus allowing comparison between different plasma setups. An optimal treatment time of 120 s was determined by taking a variation of treatment times leading up to and surpassing this and taking into account radical strength and evaporation this time was deemed most suitable. The same process for sample volume, a liquid volume great enough to avoid over evaporation but not too large so as to diminish radical strength. Spin trap concentration were maintained at either 56 mM or 100 mM during testing, as this allowed for both the RF plasma and high voltage plasma jets to produce identifiable signals.

Figures 4.1 and 4.2 were run with 100 mM DMPO, in a sample volume of 70 μl and treatment times of 120 s. Data was taken for the pulsed nanosecond plasma jet of oxygen admixtures up to 1.0 %, this highlights the effect oxygen has on the OH production in this system as well as highlighting the stability of both the power supply and the EPR spectrometer, over a repeated set of experimental data as shown in figure 4.1.

Figure 4.1 shows the $OH\cdot$ intensity as measured using a nanosecond pulsed plasma jet as a function of oxygen admixture, to observe changes over a $0 \rightarrow 1.0$ % oxygen admixture. Error was calculated through standard deviation of four sets of repeated data and a total error maximum deviation was calculated ranging from 0.6 % to 17 %. The rate of
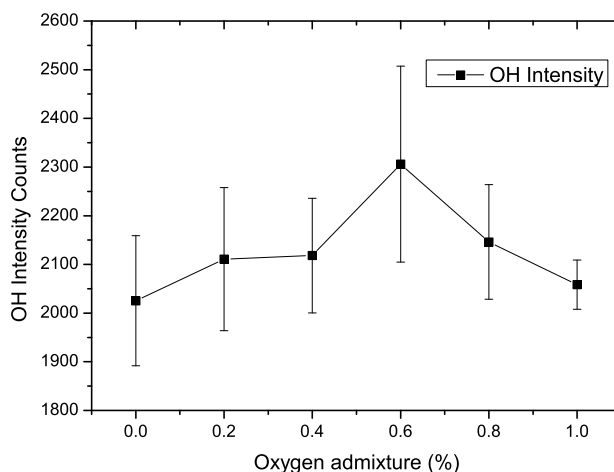
FIGURE 4.1: $OH\cdot$ intensity for different oxygen admixtures with a helium pulsed nanosecond plasma jet configuration

change of $OH\cdot$ intensity over the oxygen admixture increase doesn't suggest significant influence of oxygen on the spin trapping of $OH\cdot$.

Figure 4.2 shows the $OH\cdot$ intensity as a function of distance of the plasma nozzle from the sample, the results highlight the most effective treatment distance of the nanosecond pulsed plasma jet to the liquid interface. The closest placement of the quartz tube to the liquid surface was set at 2.5 mm, this was the optimum distance for this environment as any closer caused a take up of liquid into the quartz glass tube disturbing the plasma. With incremental distances from the treated liquid $OH\cdot$ intensity values were recorded and repeated to determine the most effective distance and chemically rich environment. The results outline the $OH\cdot$ radical strength at the various measurements with associated error suggesting that at 10 mm from the initial setup placement was the ideal environment. This raises a few points as to the influence of the local atmospheric gases in the gas phase production of $OH\cdot$. It determines the most effective $OH\cdot$ trapping distance at 12.5 mm. For most cases the radical lifetimes are short and therefore to minimise interaction with the surrounding atmospheric gases an initial assumption was to minimise local environmental interactions by holding the plasma jet close to the sample.

Due to the lack of charged species beyond the outlet of the RF plasma an active plasma is not present, but a reactive neutral effluent is [29]. This influences the alignment of the plasma and liquid interface as it is not obvious where the neutral effluent is effective to, therefore data taken by Waskoenig et al [42] details the exponential decay of atomic oxygen after it has left the nozzle of the RF plasma, this is shown in figure 4.3 which implies the closer the sample the more effective the transfer of neutrals.
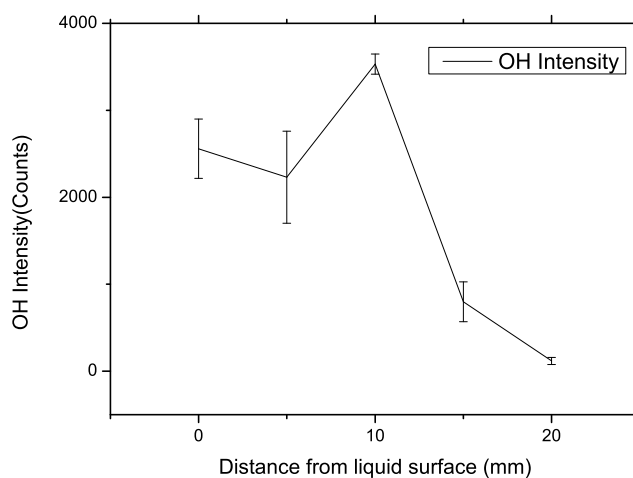
FIGURE 4.2: $OH\cdot$ intensity at increasing distances from liquid surface.
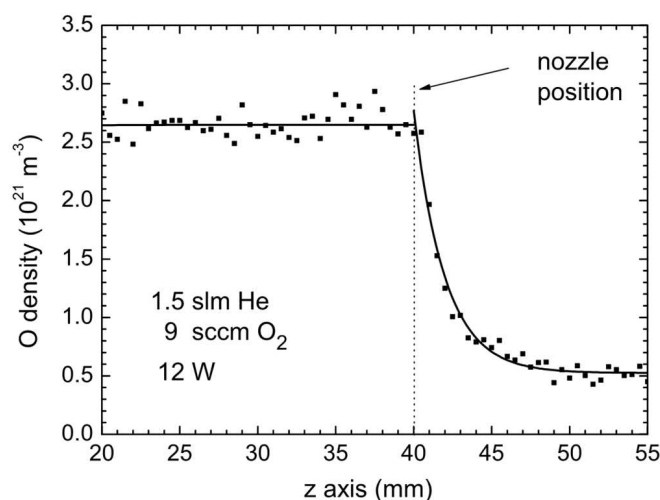
FIGURE 4.3: Data highlights an exponential decay of atomic oxygen with helium admixture once the discharge has exited the nozzle [42].

Unlike the DBD configuration, this setup requires the plasma proximity to be close, with accurate positioning over the sample, again far enough to prevent liquid uptake into the electrode set up, this distance was established at ~ 3 mm.

4.1.1   Liquid interface modification

A continuation on the plasma-liquid interaction examines how the plasma-liquid radical pathway behaves when a surfactant is placed in varying concentrations on the plasma surface and how this effects radical conversion into the liquid bulk. Sodium Dodecyl Sulphate (SDS) is a surfactant that lowers surface tension and remains settled on the surface. This experiment will monitor how radicals behave and whether they reach

the liquid bulk in the same form when a surfactant is present. It will examine how the radical concentration varies for different SDS concentration and provide comparison from a purely H_2O bulk. An initial concentration of 10 mM SDS and total liquid volume of 70 μl are the basic experimental conditions. A DMPO spin trap was used at a concentration of 56 mM and a total treatment time of 120 s, the nanosecond pulsed plasma jet had a flow rate of 2 slm and a feed gas of helium. A variety of SDS and DMPO mixtures were recorded to compare the effect it would have on the absorbency of the liquid.

Figure 4.4 is a reference spectrum for the following spectra with varying SDS percentage. It has no SDS and 56 mM DMPO. Interestingly, the data presents no hyperfines for $H\cdot$ radicals which become present in subsequent SDS spectra. The reference spectrum was analysed for signal to noise and the possibility that the signal strength of $OH\cdot$ may completely mask the presence of $H\cdot$. It was noted that the gain for the SDS present data was 5 times larger then that of the spectrum with no surfactant.
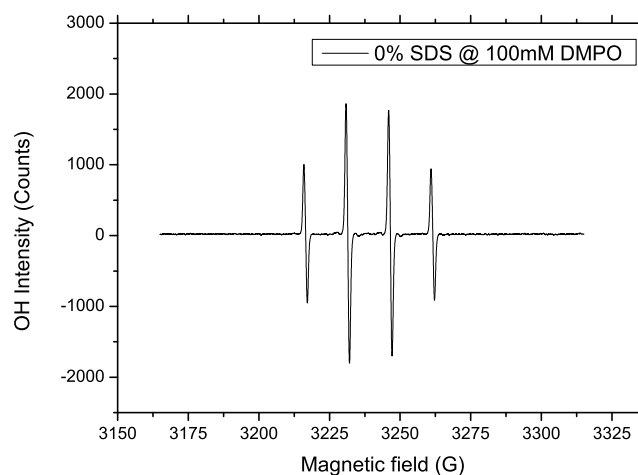
FIGURE 4.4: Reference spectrum for 56 mM DMPO with no SDS admixture.

Figure 4.5 shows spectra with an SDS percentage of 28 % at 10 mM which is the highest percentage introduced in this experiment. Signal to noise is low implying fewer $OH\cdot$ radicals are penetrating the surface. With a high surfactant percentage, the spectrum also shows radicals not present in the reference spectrum. These fit the hyperfines for $H\cdot$ radicals, and interestingly only become visible when the intensity for $OH\cdot$ is decreased. This data was obtained using the nanosecond pulsed plasma jet operating with a feed gas of helium at 2 slm, total sample volume of 70 μl and treatment time of 120 s.

Figure 4.6 with an SDS percentage of 7 % at 10 mM operating under the same conditions as previous shows a significant $OH\cdot$ intensity increase, although the $H\cdot$ radical hyperfine appears unaffected and remains at relative intensity to that of figure 4.5. This suggests
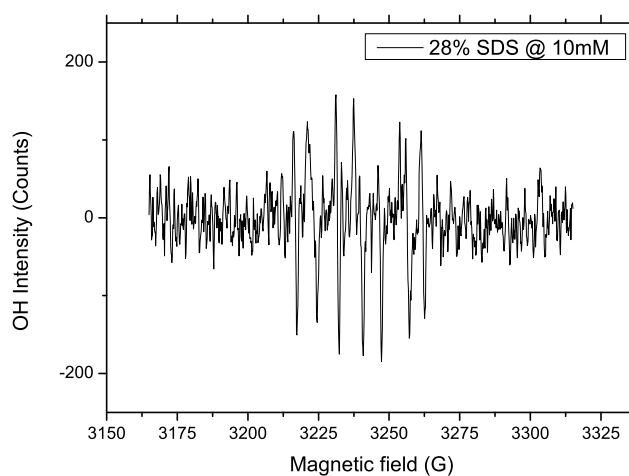
FIGURE 4.5: 28 % SDS @ 10 mM admixture with a 56 mM DMPO concentration.

the liquid interface with changing surface tension is impacting the gas phase to liquid pathway of the radical.
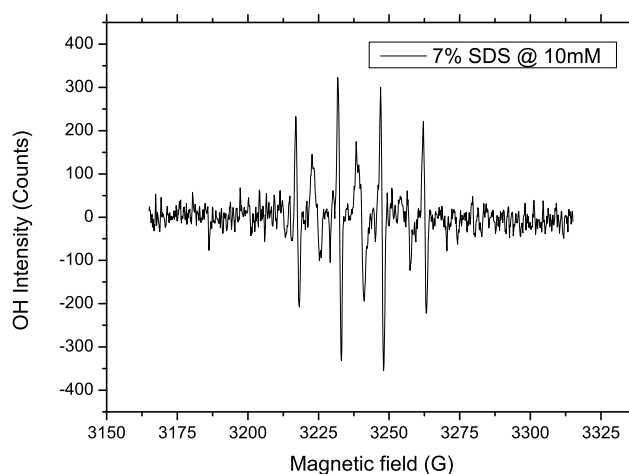
FIGURE 4.6: 7 % SDS @ 10 mM admixture with a 56 mM DMPO concentration.

To compare the 10 mM SDS solution, a second experiment was set up using all the same references but a weaker solution of 1 mM surfactant. This allows the comparison of the different states and whether the surfactant relationship can be modelled as linear.

In figure 4.7 the surfactant is reduced to a 1 mM concentration and with the same surfactant to spin trap percentage of 28 %. The signal to noise level is much lower and $H\cdot$ radicals can also be clearly seen, even with the decrease in SDS concentration the overall intensity is still far less than that of the reference spectrum. When comparing to 28 % at 10 mM SDS the signal does not have a factor of 10 difference more in the
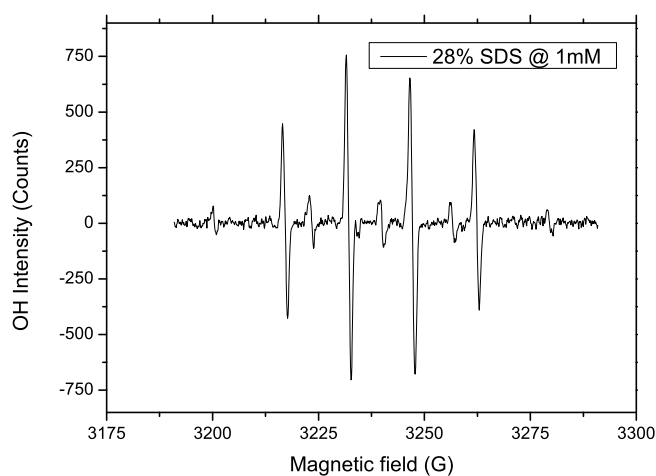
FIGURE 4.7: 28 % SDS @ 1 mM admixture with a 56 mM DMPO concentration.

region of 5. The $H\cdot$ radical signals appear largely unchanged and the emphasis is on the $OH\cdot$ radical signal that is most affected by the surfactant.
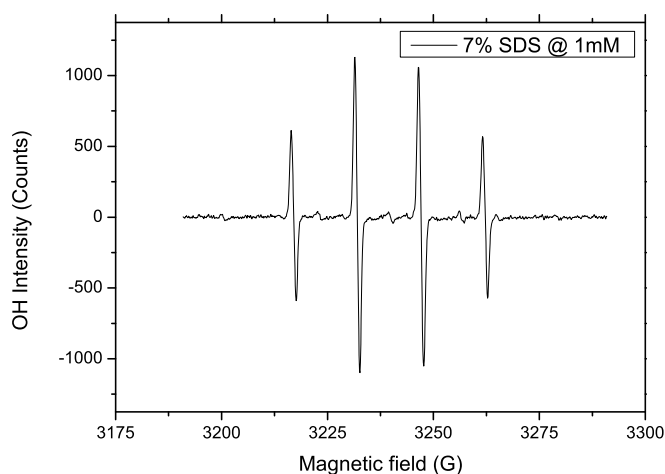
FIGURE 4.8: 7 % SDS @ 1 mM admixture with a 56 mM DMPO concentration.

Figure 4.8 the SDS percentage is only 7 % and at a concentration of 1 mM this shows a spectrum with similar profile to figure 4.4 which has no surfactant added. This leads the conclusion that $OH\cdot$ is truly affected by an introduction of SDS whereas the levels of $H\cdot$ remain constant throughout.

The data collected shows a variation in $OH\cdot$ intensity measured in the liquid that suggests $OH\cdot$ or any gas phase product capable of creating $OH\cdot$ in the liquid cannot fully be absorbed into the liquid bulk due to the change in surface tension. With the smaller $H\cdot$ signal, the final product looks to be formed from an interaction of the plasma and

liquid surface, as the figures remained unchanged with the varying SDS concentrations. This agrees with results obtained by Hase et al, that showed $H\cdot$ and $OH\cdot$ production through the dissociation of H_2O when a contact glow discharge (CGD) was applied to a liquid containing DMPO and analysed in an EPR spectrometer [26]. This does raise the question of why $H\cdot$ production does not appear to be affected by the surfactant and why only $OH\cdot$ signal is.

The next stage of plasma-liquid interactions is looking at better understanding how the plasma behaves once the chemistry has interacted with the surface of the liquid and moved onto the liquid bulk. This experiment also highlights the presence of radicals that are occurring. Using a fine charcoal powder which completely covers the liquid surface, it will be treated using a helium gas flow followed by igniting the plasma and continuing liquid surface treatment. The charcoal will be used to examine the various movements within the liquid bulk and whether the gas flow will contribute to mixing or whether there is a requirement for a stirrer to evenly distribute the reactive chemistry throughout the liquid.

The properties of helium that are relevant are its high thermal conductivity and low density. This can be an issue when using helium as a reference as it may not interact with the liquid or biological sample due to its behaviour once introduced into the atmosphere. No effect is observed pre plasma ignition on a sample held below the jet unless the liquid is in very close proximity, however post ignition the effluent is able to interact with the surface. Schlieren images taken by Sarron et al [43] explain the lack of interaction with a surface due to the mass of the gas and rapid upwards expansion. This is highly dependent on the gas flow rate and plasma jet tube size. The following experiment will examine the flow mechanism when a liquid surface is treated with the pulsed nanosecond plasma jet.

4.1.2 Flow mechanisms

The experimental method consisted of finely ground charcoal that was distributed evenly across the surface of liquid with a total volume of 10 ml contained in a glass beaker. The set up consisted of the pulsed nanosecond plasma jet with a purely helium feed gas and 6 cm outer diameter and 4 cm inner diameter quartz tube configuration. There was no sign of gas-surface or gas volume interaction pre plasma ignition. The plasma was ignited from a distance of 12.5 mm above the surface and treatment continued until all the charcoal particles had entered the liquid bulk.

Once the charcoal had mixed with the liquid bulk a flow pattern was observed, it was only present after plasma ignition and the liquid flow would cease once the plasma was

extinguished. Tests were done involving various feed gas flow rates and liquid volumes to recreate the flow without an ignited plasma. The only observable disruption from the plasma feed gas was from the liquid surface directly below the glass tube nozzle but only when the plasma was in close proximity and never enough to cause the flow patterns observed. The figure 4.9 represents the flow pattern observed with the charcoal pieces once the plasma has been ignited. This experiment helps to explain how the radicals behave once they have left the gas phase of the plasma and entered the liquid bulk. It demonstrates an even distribution of species throughout the volume of plasma treated liquid, but only if the feed gas flow rate and sample volume are matched.
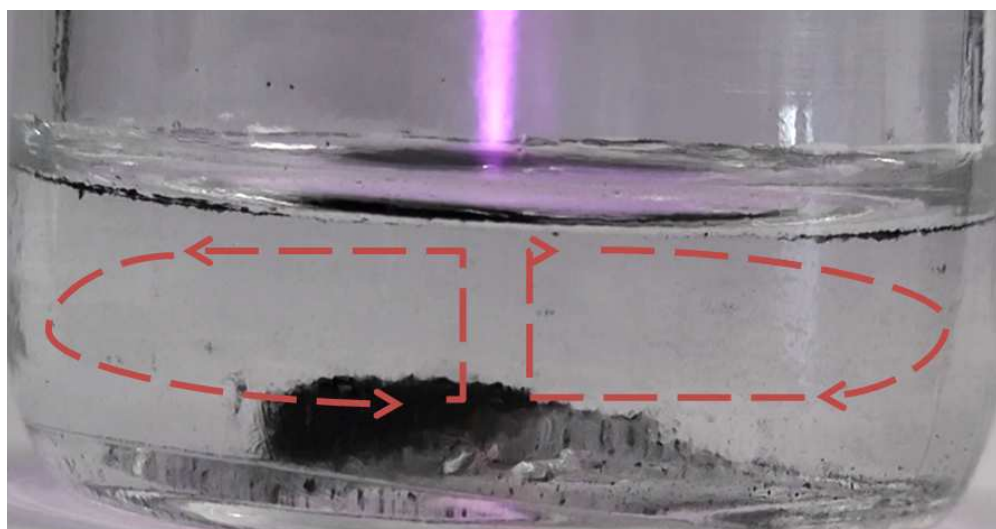
FIGURE 4.9: KHz plasma treatment of a liquid interface showing the flow mechanisms associated with the ignited plasma within the liquid

Figure 4.9 shows a liquid volume being treated by the pulsed nanosecond plasma jet. With arrow representation of the flow that is caused only when the plasma is ignited. This is interesting to observe as it suggests a liquid volume will have uniform chemistry distribution.

4.1.3 Hydrogen Peroxide in the liquid phase

Evaluation of the hydrogen peroxide levels in the 70 μ l spin trap sample liquid post plasma treatment was necessary to determine if the levels would be hazardous for cell viability, as H_2O_2 is known to be toxic in a cellular environment [44]. A colorimetric technique by Robin M Sellars was developed for sensitive peroxide levels in small volumes [23].

The principle of this technique is to measure the intensity of a yellow complex formed from the titanium (IV) oxalate and hydrogen peroxide that absorbs at a λ_{max} 400 nm. The benefits over detection strips allow this method to accurately detect H_2O_2 at low

concentrations $\geq 10\ \mu$M. Cell growth media and deionised water will be the main liquids examined for varying hydrogen peroxide concentrations under various admixtures and different plasma setups.

$$Ti^{4+} + H_2O_2 + 2H_2O \rightarrow TiO_2 \times H_2O_2 + 4H^+ \tag{4.1}$$

Equation 4.1 is the analysis of colorimetric method through H_2O_2 formation.

The titanium (IV) reagent is comprised of 5 M sulphuric acid and 0.1 M Titanium (IV) oxalate dissolved in water with Ethylenediaminetetraacetic acid (EDTA) added to stop any further reactions with transition metal that may interfere with the final concentration of hydrogen peroxide. The levels of yellowing found depended on the plasma setup, treatment time and volume of liquid. Below is the calibration curve produced using known hydrogen peroxide concentrations of 50 μM $\rightarrow$ 2 mM. Data was recorded using a UV-Visible Spectrophotometer, the data below 325 nm showing a spike, this was attributed to impurities in the Ti(IV) oxalate compound.
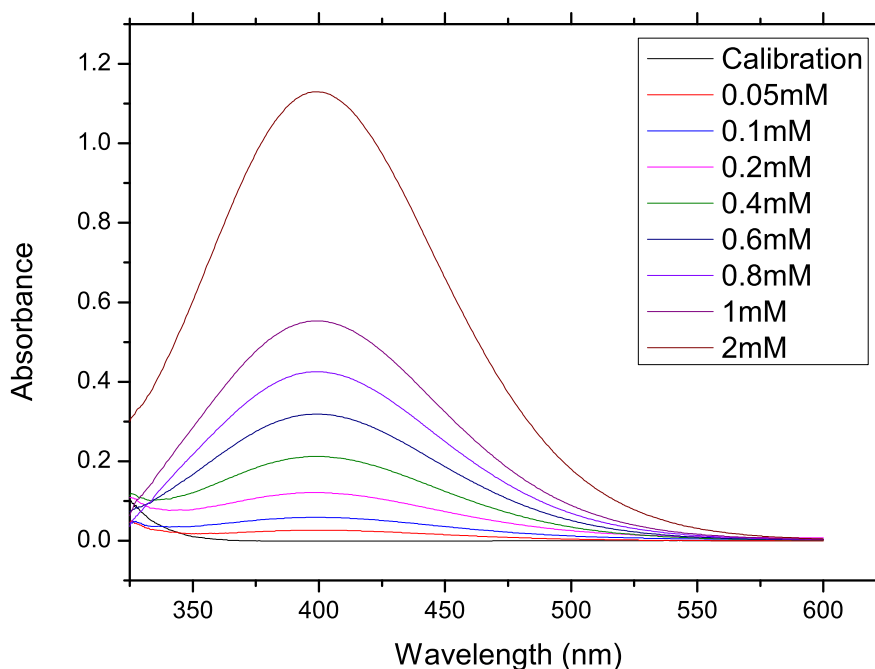
FIGURE 4.10: Data obtained using known hydrogen peroxide concentration.

Figure 4.10 is the data obtained when forming a set of calibration data to compare with plasma treated samples of the same volume.

The data was compiled and analysed depending on treatment time, a single data point taken from the 400 nm absorbance of each dataset and then plotted against its H_2O_2 concentration as shown in figure 4.11.
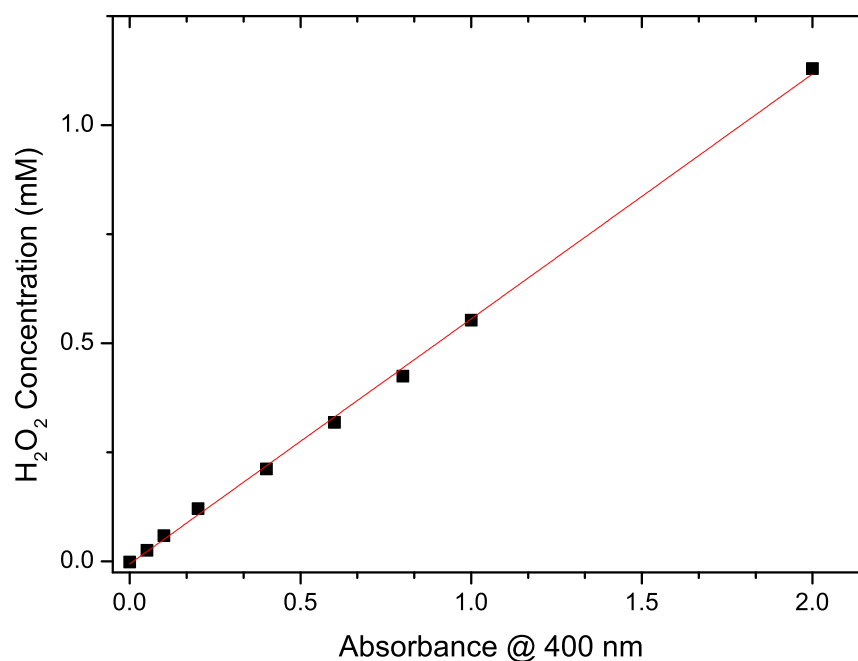
FIGURE 4.11: Calibration line obtained using λ_{max} data points at 400 nm.

Figure 4.11 gives the data calibration curve produced from the line of best fit, giving a relationship $y = mx + c$ or $A = \epsilon cl$ equating to $A = absorption$, ϵ=absorption coefficient, $c = constant$ and $l = length = 1$.

All three plasmas set-ups were operated with similar conditions to treat water and growth media (RPMI 1640 from Life Technologies, with 1 % L-Glutamine, and 5-10 % foetal calf serum) as used by collaborators in the Cancer Research Unit, Department of Biology, University of York, to compare the levels of hydrogen peroxide detected. The results will help to determine if hydrogen peroxide causes toxic levels of oxidative stress during treatment of cancerous and healthy cells. The aim is to compare three different plasma sources and regimes, these include the pulsed nanosecond plasma, the kHz sinusoidal and 13.56 MHz RF plasma. The initial testing to observe any peroxide change over time variation, sample volume or oxygen admixture were taken using the pulsed nanosecond plasma.

Figure 4.12 exhibits hydrogen peroxide concentration variation over an increasing oxygen admixtures, there is a total hydrogen peroxide fluctuation of 0.02 mM which is included in the largest error calculated for this system.
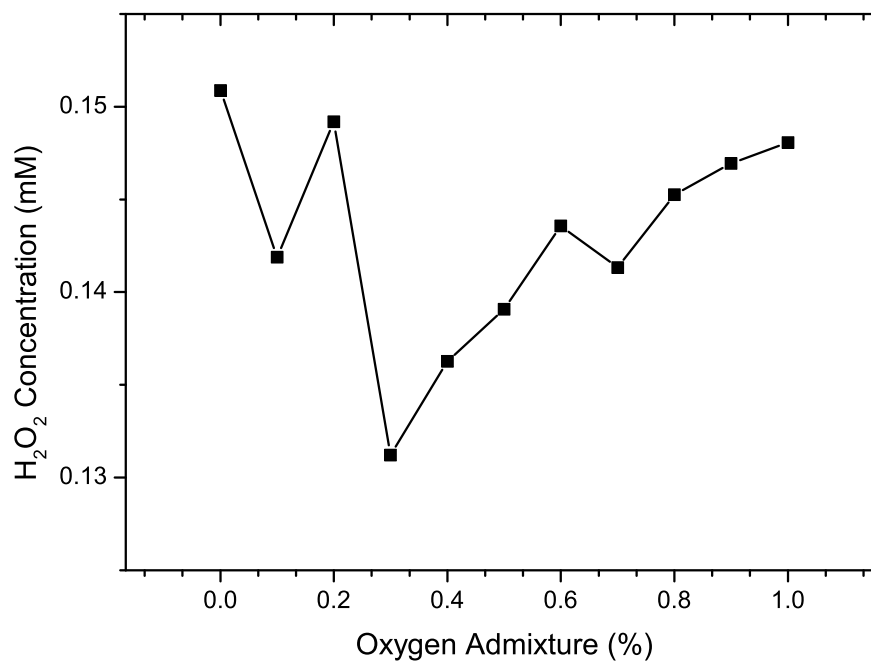
FIGURE 4.12: Variation of hydrogen peroxide over increasing oxygen admixture, when spin trap solution was treated with the pulsed nanosecond plasma.
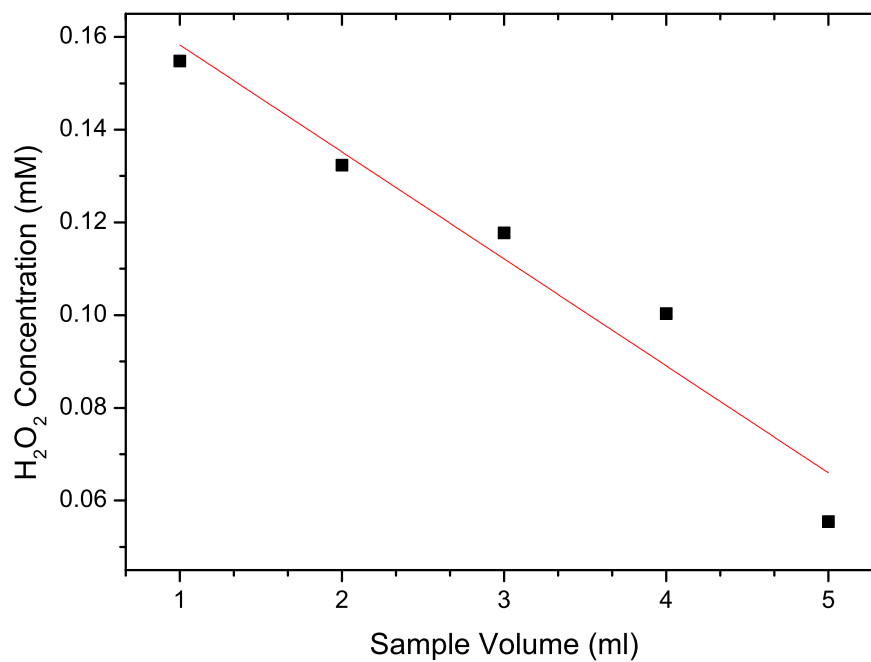
FIGURE 4.13: Variation of hydrogen peroxide over increasing sample volume when treated with a pulsed nanosecond plasma.

The data represented in figure 4.13 exhibits a linear decrease in concentration as expected for a linear increase in sample volume, starting at a value of 0.15 mM in 1 ml and ending at 5 ml of solution with a concentration of 0.06 mM. A time dependent test was produced to look at how longer plasma treatment times would affect the liquid, whether evaporation would play an important role and if the liquids pH would vary. The time scales are based on plasma treatment of cancer cells and include $0 \rightarrow 10$ min treatment times.
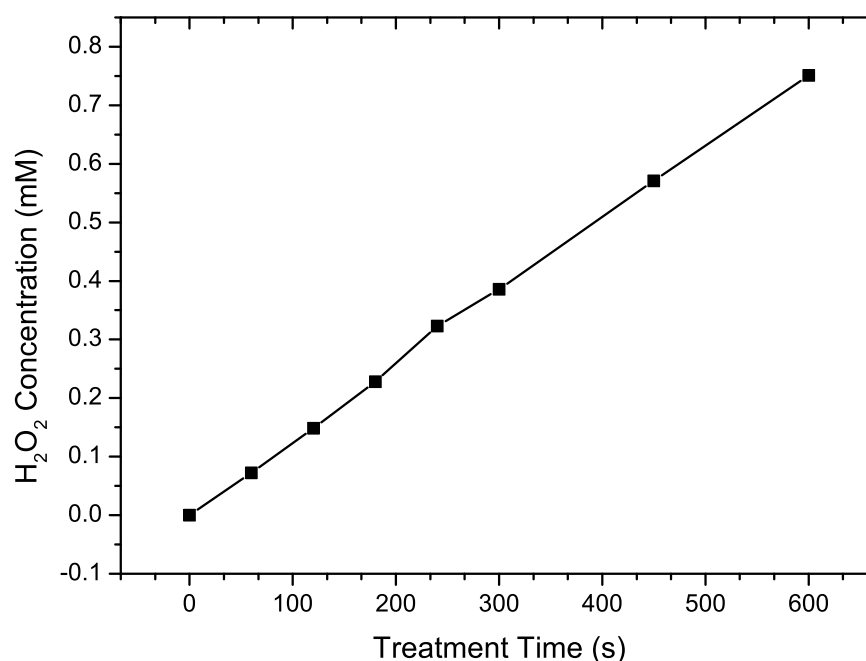
FIGURE 4.14: Hydrogen peroxide increase once treated with the pulsed nanosecond plasma over a time variation.

The relationship between an increasing treatment time and variation in hydrogen peroxide concentration as shown in figure 4.14 also demonstrates a linear relationship. The levels detected after 10 minutes of treatment 0.75 mM are high enough to cause significant oxidative stress within a biological environment. To follow this up an experiment was reproduced using Ti(IV) oxalate and a 1.5 ml sample volume with a helium feed gas and 0.3 % oxygen admixture to replicate my colleagues set up in the Cancer Research Unit.

Figure 4.15 shows the nanosecond pulsed plasma over a defined time scale against calculated H_2O_2 concentration. The results show a positive correlation, however H_2O_2 levels are severely diminished in comparison to treatment in a purely H_2O solution.

Table 4.1 shows a maximum peroxide level at a 10 min treatment time with a value of 0.75 mM and in the growth media the same treatment time gave a concentration of 0.15
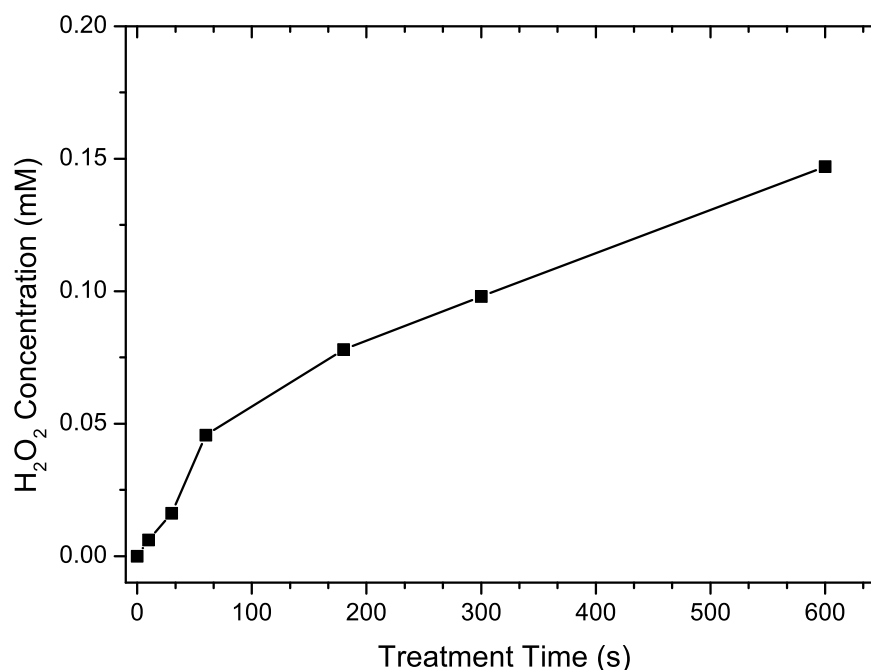
FIGURE 4.15: Variation in H_2O_2 of the pulsed nanosecond plasma in a growth media environment.

mM, this is a significant decrease, however the growth media has a very complex set of additives, also noted is the higher viscosity of the growth media which may play an important role.

Figure 4.16 gives concentration against treatment time values for hydrogen peroxide levels in growth media after treatment with the sinusoidal kHz plasma. As observed from table 4.1 the level was 0.072 mM after a 10 min plasma treatment, which coincides with the maximum time biological samples are treated for in the Cancer Research Unit, however the final hydrogen peroxide level is 4 times weaker than the pulsed nanosecond sample resulting in an overall milder dose experienced by the treated sample. To put this in perspective significant cell death can be observed when a reference concentration of H_2O_2 at 1 mM is applied to biological samples alongside plasma treatment [45].

The final plasma set-up investigated was the 13.56 MHz Radio frequency (RF) power supply maintaining the same flow rate and admixture as well as treatment time.

The results from the 13.56 MHz plasma jet as shown in figure 4.17 demonstrate how much lower yet consistent the results are compared with a purely H_2O sample and the two previous plasma jet setups. The 10 min treatment shows a concentration of 0.031 mM as compared to a water sample of 0.007 mM, the results for water were much more erratic and required constant reiteration of the baseline on the UV-Visible spectrophotometer
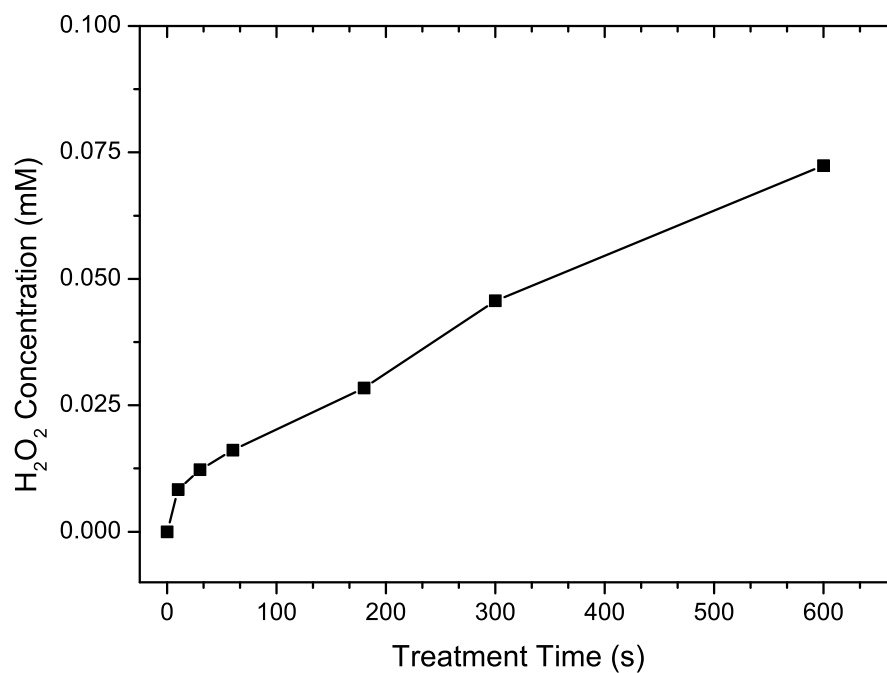
FIGURE 4.16: Variation in H_2O_2 of the sinusoidal plasma in a growth media environment.
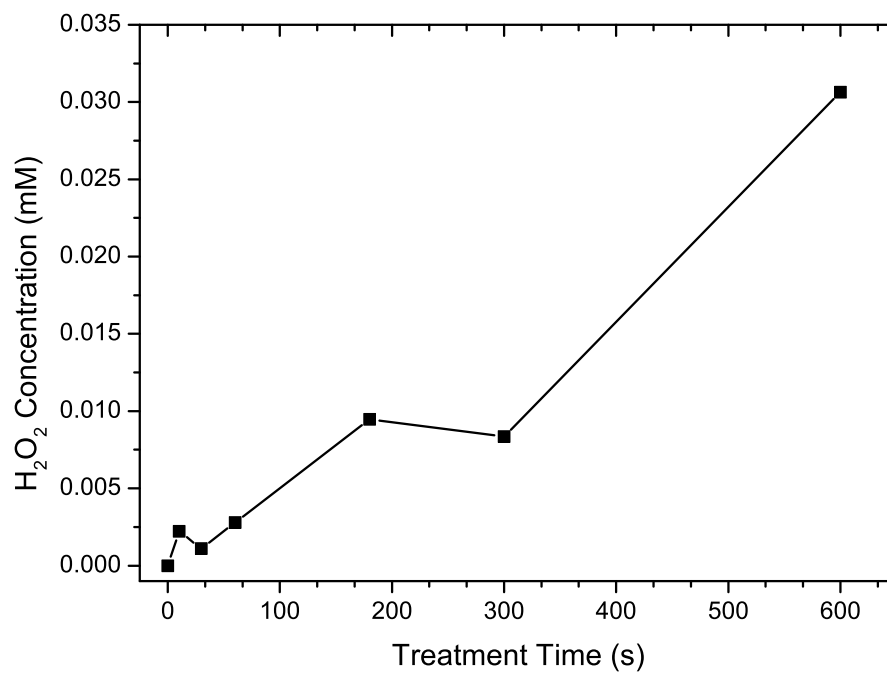
FIGURE 4.17: 13.56 MHz radio frequency plasma variation of H_2O_2 in a growth media environment.

between each sample, this suggests the growth media is a stable environment despite not absorbing as much H_2O_2.

Table 4.1 below shows values for all data points taken on the three different plasma setups. All used a feed gas of helium and oxygen admixture of 0.3 %, a sample volume of 1.5 ml.

TABLE 4.1: Comparison of percentages.

	Nano-second		Sinusoidal		RF	
Time	H_2O	Media	H_2O	Media	H_2O	Media
(s)	(mM)	(mM)	(mM)	(mM)	(mM)	(mM)
10	0.008	0.006	0.006	0.008	0.001	0.002
30	0.034	0.016	0.002	0.012	0.001	0.001
60	0.072	0.046	0.003	0.016	0.017	0.003
180	0.228	0.078	0.019	0.028	0.009	0.009
300	0.571	0.098	0.018	0.046	0.010	0.008
600	0.751	0.147	0.037	0.072	0.007	0.031

In conclusion this work produced interesting comparisons between the H_2O and RPMI 1640 growth media. It highlights a less concentrated H_2O_2 sample is found in growth media, but with a more stable H_2O_2 relationship.

4.1.4 RF spin trapping

Investigating the effects of $OH\cdot$ production over an oxygen admixture range of 0 - 1.0 % using a 13.56 MHz and 40.68 MHz RF plasma. This work was carried out to investigate the rate of $OH\cdot$ production on a better modelled system over two frequency ranges. Spectra show a very large variation of $OH\cdot$ intensity over the 0 - 1.0 % admixture range. With large associated error calculated from repeats. The DMPO concentration was increased to 100 mM due to the weaker $OH\cdot$ obtained from the RF setup.

Figure 4.18 examines the relationship between $OH\cdot$ production as a function of oxygen admixture. The 13.56 MHz signal has a more stable overall signal with smaller associated error whereas the 40.68 MHz data shows a decrease in $OH\cdot$ production with increasing oxygen. This agrees with the non apparent relationship between gas phase to liquid bulk conversion of $OH\cdot$ production found in the nanosecond plasma jet configuration. Work done by Knake et al [46] shows an oxygen density peak at 0.5 - 0.6 % when measuring in the gas phase using TALIF. This relationship did not continue onto the liquid phase. In both the 13.56 and 40.68 MHz plasmas the purely helium feed gas with no oxygen admixture gave the highest $OH\cdot$ signal, which confirms the oxygen admixture does not have as great an impact on $OH\cdot$ conversion to the liquid bulk as anticipated.
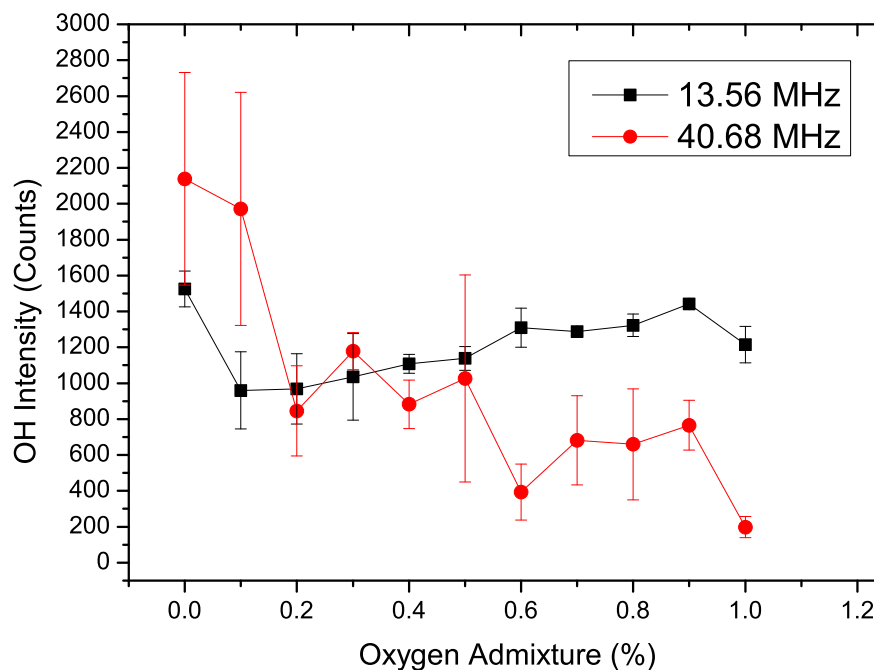
FIGURE 4.18: 13.56 MHz radio frequency vs 40.68 MHz $OH\cdot$ production in DMPO spin trap, as a function oxygen admixtures.

4.1.5 Spin trapping DEPMPO

The work with spin traps has been exclusively DMPO however DEPMPO was also investigated to help develop a complete picture when examining radicals present in the liquid environment. DEPMPO has a much more stable adduct for $O_2^{\cdot-}$ to allow it to be trapped and imaged. The spectrum produced retains a lot of information trapped by various radicals, complicating the spectrum. Figure 4.19 is the spectra taken from the pulsed nanosecond plasma treating 50 μl of DEPMPO solution at 100 mM concentration. The signal to noise ratio is high giving a clean set of spectra, this allowing for fewer sweeps of the sample by the EPR spectrometer and retaining a stronger radical signal. The radicals detected within this spectrum are the same as previously discussed in 3.4. However due to the concentration of the DEPMPO being doubled the signal to noise is greater.

Figure 4.19 is a spectrum of the DEPMPO intensity of all trapped radicals as a function of position in a magnetic field. The data confirms the presence of $OH\cdot$ and $O_2^{\cdot-}$ which play a key role in biomedicine. The second set of DEPMPO data as shown in figure 4.20 is produced with similar operation and sample parameters, however plasma setup is closer to the liquid surface.
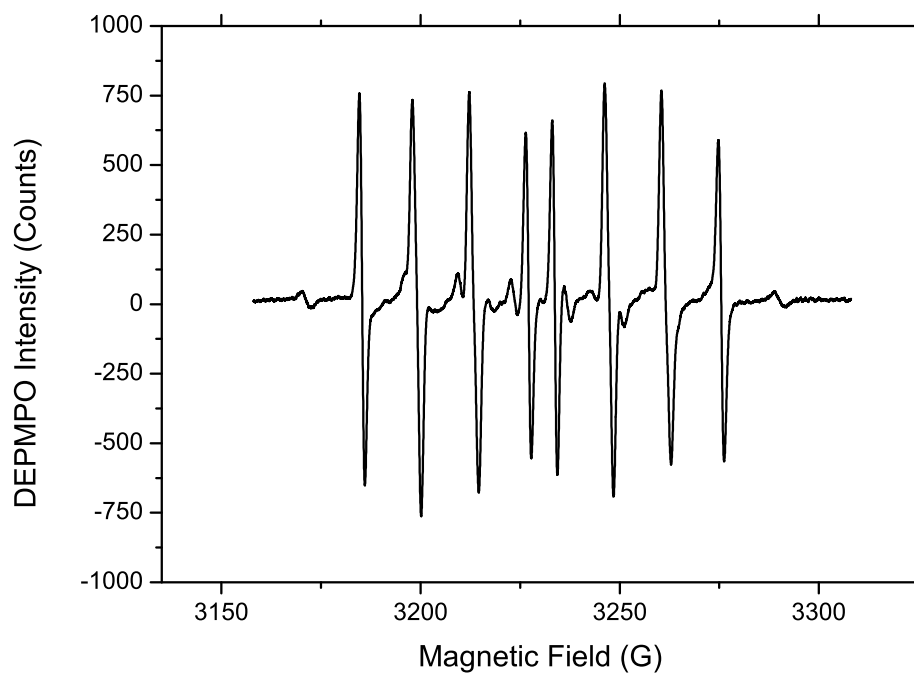
FIGURE 4.19: Spectrum for the pulsed nanosecond plasma with the use of DEPMPO as a spin trap.
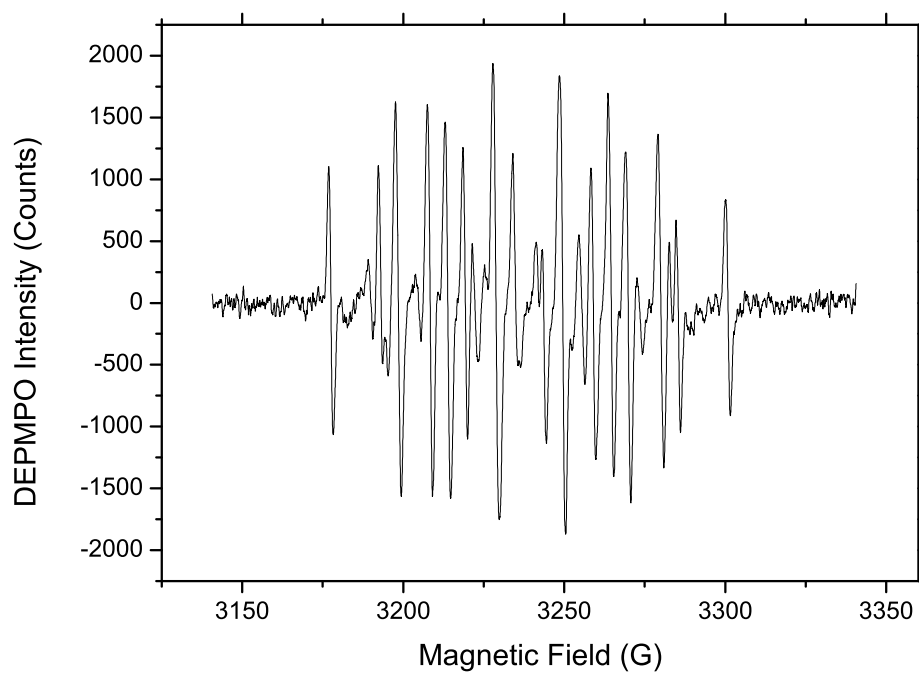
FIGURE 4.20: Spectrum for the Radio Frequency supply with the aid of DEPMPO as a spin trap.

Figure 4.20 is a spectrum obtained when treating a 50 μl liquid sample with RF plasma and 100 mM DEPMPO. This dataset has similar structure and signal strength to figure 3.12. This suggests the diminished signal strength is due to the a less effective gas phase to liquid bulk radical conversion in the RF plasma setup.

4.2   Self-assembled monolayers

The aim of treating gold-coated SAM plates with the plasma was to examine and improve on the current cleaning method that left the chip redundant after three washes.

The results from preliminary experiments showed a partial cleaning of the organic mono-layer from the chip surface, the results suggest a more desirable cleaning environment is produced when the oxygen admixture is 0.5 %.
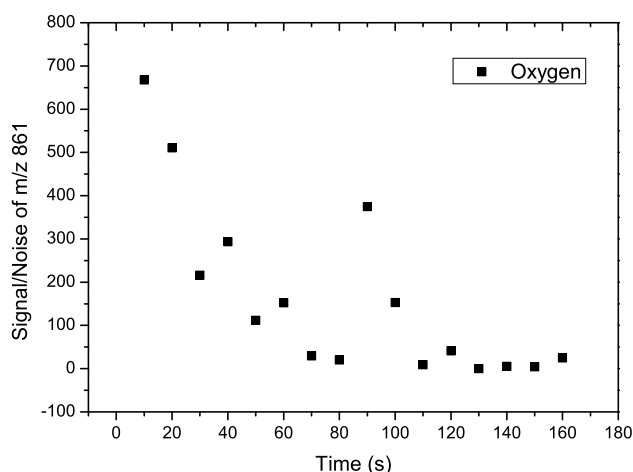
FIGURE 4.21: Plot showing the S/N of m/z 861 after wells were submitted to the plasma beam of the pulsed nanosecond plasma jet for increasing 10 s increments.

Figure 4.21 shows data analysed when treated with the pulsed nanosecond plasma jet after consecutive 10 s treatment times. The decrease in the m/z of the 861 signal suggests the surface is being cleaned. For a more accurate conclusions multiple repeats and variations would have to be considered. The final treated surface was then re-spotted with the SAM and examined to see if the surface was clean and reusable. Data collected suggested the surface was usable and allowed for successive treatments to be done on the same plate.

Figure 4.22 shows monolayers without a matrix which are treated using the RF jet. The experiment highlights the ideal gas mixtures of nitrogen and oxygen were 0.25 % and
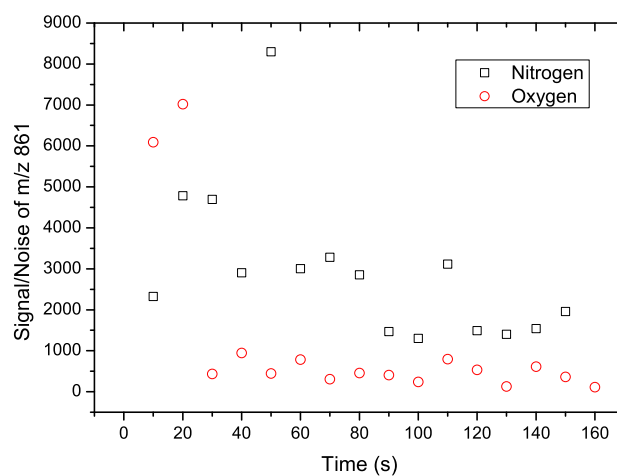
FIGURE 4.22: Plot showing signal/noise of m/z 861 at increasing time points of 10 seconds after subjecting consecutive wells to cleaning with the plasma beam. Results are shown for single analyses with addition of 0.25 % nitrogen or 0.5 % oxygen.

0.5 % respectively, however when compared the preferred admixture is oxygen. These results were more consistent than data recorded using the nanosecond plasma jet.

In conclusion this method was successful in terms of re-spotting a monolayer on a plasma cleaned surface, however proper inspection of the gold surface post treatment would be necessary to determine any damage to the gold surface, this could be done by atomic force microscopy (AFM) to give a more detailed analysis.

Chapter 5

Conclusions and Future Work

The aim of this project was to further investigate the interaction of plasma created reactive species with a liquid interface and examine the following interactions that occur within the liquid bulk. A comparison was made between the two plasma jets, a DBD configuration operating with a nanosecond pulsed power supply, a DBD configuration with a sinusoidal power supply, and a capacitively coupled RF plasma.

Results highlight a selection of radicals are produced within a variety of plasma jets and associated conditions. The reactive species present included ozone (O_3), hydroxyl radical ($OH\cdot$), superoxide radical (O_2^-) and when introduced to a liquid environment hydrogen peroxide (H_2O_2) and hydrogen radical ($H\cdot$) were also detected. A spin trap solution of 100 mM was sufficient to obtain strong radical hyperfines on all plasmas, the nanosecond pulsed plasma jet consistently produced the strongest signals across the range of spin traps, this was also observed at lower spin trap solutions. The majority of experiments used $OH\cdot$ as a comparison point due to its continued presence in a liquid environment.

The strongest H_2O_2 signals were detected after longer treatment times, the 10 minute treatment was the upper limit and corresponds to the longest time used in the Cancer Research Unit under these conditions. The strongest signals detected in a liquid environment were (0.75 mM in H_2O and 0.15 mM in growth media) using the nanosecond plasma jet supply and the weakest signals and concentrations were obtained when operating the 13.56 MHz RF plasma (0.007 mM in H_2O and 0.031 mM in growth media), both these results refer to 10 minute treatment times. The H_2O_2 relationship was linear for the nanosecond DBD plasma jet in H_2O, however due to the complex growth media it represents a polynomial fit for treatment times up to 10 minutes. For the RF plasma the more stable H_2O_2 results were achieved in the growth media, due to the small non

linear concentrations detected in H_2O no relationship was observed.

Future work would require an intermediate step such as a less complex PBS solution to observe H_2O_2 change.

All the plasma sources examined produced an acidic environment post treatment. The RF source had an initial pH decrease from 5.5 but remained constant at ~3.6. Alternatively both the DBD sources decreased steadily over the 10 minute treatment reaching a final pH of ~2.6.

Surfactants applied to the liquid surface in varying concentrations showed a decrease in gas phase radicals detected in the liquid. However the small $H\cdot$ signal appeared largely unaffected by the SDS, suggesting a small number of radicals are trapped through dissociation at the liquid surface [26].

Flow mechanisms within a plasma treated bulk occur and are driven by the plasmas interaction with the liquid surface. Feed gas flow has minimal surface disturbance and the rate at which the flow starts and stops implies it cannot be thermal properties. This could also be applied to a variety of different liquids to observe rates and flow patterns. This is important in understanding how treatment of cells in solutions occurs and whether additional sample spinning is required. A computational model would pair well with this and allow for a variety of surface structures and solutions.

The spin trapping of nitrogen in a helium plasma can also be applied in the same way as described for oxygen. Only a small proportion of this investigation considered nitrogen species in the liquid, future work is envisaged to also consider these nitrogen species, such as nitric oxide (NO), given its immense biological importance.

Research into the effects of electrons interacting with liquid surfaces would allow further modelling of the kHz DBD jet, direct comparison with the RF jet would highlight the importance of hydrated electrons in a variety of liquids and setup parameters.

As observed with the organic monolayer surface cleaning it is the selectivity of reactive species and tailoring to the application that is key. Adjusting the electrode configurations on the DBD plasma would allow further optimisation of the plasma conditions as well as plasma geometry.

References

[1] I. Langmuir. Oscillations in ionized gases. *Proc. Natl. Acad. Sci, U.S.A.*, 14 (8): 628, 1928.

[2] Davide Mariotti, Jenish Patel, Vladimir Svrcek, and Paul Maguire. Plasma liquid interactions at atmospheric pressure for nanomaterials synthesis and surface engineering. *Plasma Processes and Polymers*, 9(11-12):1074–1085, 2012.

[3] Mahmoud Y. Alkawareek, Qais Th. Algwari, Garry Laverty, Sean P. Gorman, William G. Graham, Deborah O'Connell, and Brendan F. Gilmore. Eradication of pseudomonas aeruginosa biofilms by atmospheric pressure non-thermal plasma. *PLoS ONE*, 7(8):e44289, 08 2012.

[4] K Niemi, J Waskoenig, N Sadeghi, T Gans, and D O'Connell. The role of helium metastable states in radio-frequency driven heliumoxygen atmospheric pressure plasma jets: measurement and numerical simulation. *Plasma Sources Science and Technology*, 20(5):055005, 2011.

[5] V Schulz von der Gathen, L Schaper, N Knake, S Reuter, K Niemi, T Gans, and J Winter. Spatially resolved diagnostics on a microscale atmospheric pressure plasma jet. *Journal of Physics D: Applied Physics*, 41(19):194004, 2008.

[6] XinPei Lu and Mounir Laroussi. Dynamics of an atmospheric pressure plasma plume generated by submicrosecond voltage pulses. *Journal of Applied Physics*, 100(6):063302, 2006.

[7] J L Walsh, P Olszewski, and J W Bradley. The manipulation of atmospheric pressure dielectric barrier plasma jets. *Plasma Sources Science and Technology*, 21 (3):034007, 2012.

[8] E Wagenaars, T Gans, D O'Connell, and K Niemi. Two-photon absorption laser-induced fluorescence measurements of atomic nitrogen in a radio-frequency atmospheric-pressure plasma jet. *Plasma Sources Science and Technology*, 21(4): 042002, 2012.

[9] D. Maletic, N. Puac, S. Lazovic, G. Malovic, T. Gans, V. Schulz-von der Gathen, and Z. Lj Petrovic. Detection of atomic oxygen and nitrogen created in a radio-frequency-driven micro-scale atmospheric pressure plasma jet using mass spectrometry. *Plasma Physics and controlled fusion*, 54(12), 2012.

[10] Tomoyuki Murakami, Kari Niemi, Timo Gans, Deborah O'Connell, and William G Graham. Interacting kinetics of neutral and ionic species in an atmospheric-pressure heliumoxygen plasma with humid air impurities. *Plasma sources science & technology*, 22(4), 2013.

[11] Jochen Waskoenig, Kari Niemi, Nikolas Knake, Lucy Marie Graham, Stephan Reuter, Volker Schulz-von der Gathen, and Timo Gans. Diagnostic-based modeling on a micro-scale atmospheric-pressure plasma jet. *Pure and applied chemistry*, 82 (6):1209–1222, 2010.

[12] K. Niemi, S. Reuter, L. M. Graham, J. Waskoenig, and T. Gans. Diagnostic based modeling for determining absolute atomic oxygen densities in atmospheric pressure helium-oxygen plasmas. *Applied Physics Letters*, 95(15):151504, 2009.

[13] David B Graves. The emerging role of reactive oxygen and nitrogen species in redox biology and some implications for plasma applications to medicine and biology. *Journal of Physics D: Applied Physics*, 45(26):263001, 2012.

[14] Marilia T. C. Martins-Costa, Josep M. Anglada, Joseph S. Francisco, and Manuel F. Ruiz-Lopez. Reactivity of atmospherically relevant small radicals at the air water interface. *Angewandte Chemie International Edition*, 51(22):5413–5417, 2012.

[15] M G Kong, M Keidar, and K Ostrikov. Plasmas meet nanoparticles where synergies can advance the frontier of medicine. *Journal of Physics D: Applied Physics*, 44 (17):174018, 2011.

[16] Atsushi Tani, Yusuke Ono, Satoshi Fukui, Satoshi Ikawa, and Katsuhisa Kitano. Free radicals induced in aqueous solution by non-contact atmospheric-pressure cold plasma. *Applied physics letter*, 100(25), JUN 18 2012.

[17] Seiji Samukawa, Masaru Hori, Shahid Rauf, Kunihide Tachibana, Peter Bruggeman, Gerrit Kroesen, J Christopher Whitehead, Anthony B Murphy, Alexander F Gutsol, Svetlana Starikovskaia, Uwe Kortshagen, Jean-Pierre Boeuf, Timothy J Sommerer, Mark J Kushner, Uwe Czarnetzki, and Nigel Mason. The 2012 plasma roadmap. *Journal of Physics D: Applied Physics*, 45(25):253001, 2012.

[18] Peter Bruggeman and Christophe Leys. Non-thermal plasmas in and in contact with liquids. *Journal of Physics D: Applied Physics*, 42(5):053001, 2009.

[19] Carl Nathan and Aihao Ding. Nonresolving inflammation, March 2010.

[20] Frederick A. Villamena, John K. Merle, Christopher M. Hadad, and Jay L. Zweier. Superoxide radical anion adduct of 5,5-dimethyl-1-pyrroline n-oxide (dmpo). 2. the thermodynamics of decay and epr spectral properties. *The Journal of Physical Chemistry A*, 109(27):6089–6098, 2005.

[21] John M.C Gutteridge Barry Haliwell. *Free radicals in biology and medicine*. Oxford University press, 2007.

[22] Satoshi Ikawa, Katsuhisa Kitano, and Satoshi Hamaguchi. Effects of ph on bacterial inactivation in aqueous solutions due to low-temperature atmospheric pressure plasma application. *Plasma Processes and Polymers*, 7(1):33–42, 2010.

[23] Robin M. Sellers. Spectrophotometric determination of hydrogen peroxide using potassium titanium(iv) oxalate. *Analyst*, 105:950–954, 1980.

[24] K. Oehmigen, M. Hhnel, R. Brandenburg, Ch. Wilke, K.-D. Weltmann, and Th. von Woedtke. The role of acidification for antimicrobial activity of atmospheric pressure plasma in liquids. *Plasma Processes and Polymers*, 7(3-4):250–257, 2010.

[25] Henry Jay Forman, Jon M. Fukuto, Tom Miller, Hongqiao Zhang, Alessandra Rinna, and Smadar Levy. The chemistry of cell signaling by reactive oxygen and nitrogen species and 4-hydroxynonenal. *Archives of Biochemistry and Biophysics*, 477(2):183 – 195, 2008.

[26] Hirotomo Hase and Kaoru Harada. Esr detection of oh and h radicals generated by contact glow discharge in aqueous solutions. *http://www.origin-life.gr.jp/*, 2001.

[27] Alexander Fridman. *Plasma Chemistry*. Cambridge, 2008.

[28] Eisuke Takai, Satoshi Ikawa, Katsuhisa Kitano, Junpei Kuwabara, and Kentaro Shiraki. Molecular mechanism of plasma sterilization in solution with the reduced ph method: importance of permeation of hoo radicals into the cell membrane. *Journal of Physics D: Applied Physics*, 46(29):295402, 2013.

[29] J. S. Sousa, K. Niemi, L. J. Cox, Q. Th. Algwari, T. Gans, and D. OConnell. Cold atmospheric pressure plasma jets as sources of singlet delta oxygen for biomedical applications. *Journal of Applied Physics*, 109(12):123302, 2011.

[30] A. A. Frimer and L. M. Stephenson. *Singlet Oxygen*. CRC Press, 1985.

[31] Matthew J Pavlovich, Hung-Wen Chang, Yukinori Sakiyama, Douglas S Clark, and David B Graves. Ozone correlates with antibacterial effects from indirect air dielectric barrier discharge treatment of water. *Journal of Physics D: Applied Physics*, 46(14):145202, 2013.

[32] V Kudrle, P Vaina, A Tlsk, M Mrzkov, O tec, and J Jana. Plasma diagnostics using electron paramagnetic resonance. *Journal of Physics D: Applied Physics*, 43 (12):124020, 2010.

[33] Elio Giamello Marina Brustolon, editor. *Electron Paramagnetic Resonance: A Practitioners Toolkit.* Wiley, 2009.

[34] Klaus Stolze, Natascha Rohr-Udilova, Thomas Rosenau, Roswitha Stadtmller, and Hans Nohl. Very stable superoxide radical adducts of 5-ethoxycarbonyl- 3,5-dimethyl-pyrroline n-oxide (3,5-edpo) and its derivatives. *Biochemical Pharmacology*, 69(9):1351 – 1361, 2005.

[35] Garry R. Buettner. Spin trapping: Esr parameters of spin adducts. *Free Radical Biology and Medicine*, 3(4):259 – 303, 1987.

[36] Tor Arne Vestad. *ESR spin trapping.* PhD thesis, University of Oslo, 1993.

[37] Jean-Louis Clement, Nicolas Ferre, Didier Siri, Hakim Karoui, Antal Rockenbauer, and Paul Tordo. Assignment of the epr spectrum of 5,5-dimethyl-1-pyrroline n-oxide (dmpo) superoxide spin adduct. *The Journal of Organic Chemistry*, 70(4): 1198–1203, 2005. PMID: 15704951.

[38] I. Jonathan Amster. Fourier transform mass spectrometry. *Journal of Mass Spectrometry*, 31(12):1325–1337, 1996.

[39] Alan G. Marshall, Christopher L. Hendrickson, and George S. Jackson. Fourier transform ion cyclotron resonance mass spectrometry: A primer. *Mass Spectrometry Reviews*, 17(1):1–35, 1998.

[40] K. Niemi, C. O'Neill, L. J. Cox, J. Waskoenig, W. B. Hyland, S. J. McMahon, S. Reuter, F. J. Currell, W. G. Graham, D. O'Connell, and T. Gans. Cold atmospheric pressure plasma jets: Interaction with plasmid dna and tailored electron heating using dual-frequency excitation. *AIP Conference Proceedings*, 1438(1):23–28, 2012.

[41] S. Singh and R.C. Hider. Colorimetric detection of the hydroxyl radical: Comparison of the hydroxyl-radical-generating ability of various iron complexes. *Analytical Biochemistry*, 171(1):47 – 54, 1988.

[42] J Waskoenig, K Niemi, N Knake, L M Graham, S Reuter, V Schulz von der Gathen, and T Gans. Atomic oxygen formation in a radio-frequency driven micro-atmospheric pressure plasma jet. *Plasma Sources Science and Technology*, 19(4): 045018, 2010.

[43] J. Fontane T. Darny D. Ris S. Dozias L. Joly V. Sarron, E. Robert and J.M. Pouvesle. Plasma plume length characterization. 2013.

[44] RE. Lewellyn AL. Pierce, GB. Parchment. Hydrogen peroxide as a mediator of programmed cell death in the blastocyst. *PMID: 1655543*, 46(3)::181–6, April 1991.

[45] Adam Hirst. Private communication. Cancer Research Unit, October 2013.

[46] Nikolas Knake, Kari Niemi, Stephan Reuter, Volker Schulz-von der Gathen, and Jorg Winter. Absolute atomic oxygen density profiles in the discharge core of a microscale atmospheric pressure plasma jet. *Applied Physics Letters*, 93(13):131503, 2008.